Estimating degree-day factors based on energy flux components

Muhammad Fraz Ismail [1, 2], Wolfgang Bogacki [2], Markus Disse [1], Michael Schäfer [2,3] and Lothar Kirschbauer [2]

5   [1]   TUM School of Engineering and Design, Technical University of Munich, Germany

       [2]   Department of Civil Engineering, Koblenz University of Applied Sciences, Germany

       [3]   Faculty of Agriculture, Yamagata University, Tsuruoka, Japan

       Correspondence: Muhammad Fraz Ismail (fraz.ismail@tum.de; ismail@hs-koblenz.de)

10   **Abstract**

Melt water from snow and ice dominated mountainous catchments is a valuable source of fresh water in many regions. Seasonal snow cover and glaciers act like a natural reservoir by storing precipitation during winter and releasing it in spring and summer. Snowmelt runoff is usually modelled either by energy balance or by temperature-index approaches. The energy balance approach is process-based and

15   more sophisticated but requires extensive input data, while the temperature-index approach uses the degree-day factor (*DDF*) as key parameter to estimate melt merely from air temperature. Despite its simplicity, the temperature-index approach has proved to be a powerful tool for simulating the melt process especially in large and data scarce catchments.

The present study attempts to quantify the effects of spatial, temporal, and climatic conditions on the

20   *DDF*, in order to gain a better understanding which influencing factors are decisive under which conditions. The analysis is physically based on the individual energy flux components, however approximate formulas for estimating the *DDF* are presented to account for situations where observed data is limited. A detailed comparison between observed and estimated *DDF* values yielded a fair agreement with BIAS= 0.2 mm °C^{-1} d^{-1} and RMSE=1.1 mm °C^{-1} d^{-1}.

25   The analysis of the energy balance processes controlling snowmelt indicates that cloud cover and under clear sky snow albedo are the most decisive factors for estimating the *DDF*. The results of this study further underline that the *DDF* changes as the melt season progresses and thus also with altitude, since melting conditions arrive later at higher elevations. A brief analysis of the *DDF* under the influence of climate change shows that the *DDFs* are expected to decrease when comparing periods of similar

30   degree-days, as melt will occur earlier in the year and albedo is then likely to be higher. Therefore, the *DDF* cannot be treated as a constant parameter especially when using temperature-index models for forecasting present or predicting future water availability.

Keywords: Degree-Day Factor, Snowmelt, Energy balance, Temperature-Index, Climate change

1. Introduction

Melt water from snow and ice dominated mountainous basins is a unique source of fresh water in many regions. Seasonal snow cover and glaciers act as natural reservoirs which significantly affect catchment hydrology by temporarily storing and releasing water on various time scales (Jansson et al., 2003). In such river basins, snow and glacier melt runoff modelling is a valuable tool when predicting downstream river flow regimes, as well as when assessing the changes in the cryosphere associated with climate change (Hock, 2003). Therefore, a most accurate quantification of the melt processes and related parameters is the key to a successful runoff modelling for the prediction of present and future water availability.

Two different approaches are common in snowmelt runoff modelling. The energy balance approach is process-based however data-intensive, since melt is deduced from the balance of in- and outgoing energy components (Braithwaite, 1995; Arendt and Sharp, 1999). On the contrary, temperature-index or also-called degree-day models merely use the air temperature as an index to assess melt rates (Martinec, 1975; Bergström, 1976; Quick and Pipes, 1977; DeWalle and Rango, 2008). The relationship between temperature and melt is defined by the degree-day factor (*DDF*) (Braithwaite, 2008), which is the amount of melt that occurs per unit positive degree-day (Braithwaite, 1995; Kayastha et al., 2003; Martinec et al., 2008). There are different methods by which the *DDF* can be determined, e.g. by measurements using ablation stakes (Zhang et al., 2006), using snow lysimetric outflows (Kustas et al., 1994), by estimating daily changes in the snow water equivalent (Martinec, 1960; Rango and Martinec, 1979, 1995; Kane et al., 1997), or using satellite based snow cover data (Asaoka and Kominami, 2013; He et al., 2014).

Because sufficient direct observations are typically lacking in large catchments, the *DDF* is usually treated as a decisive parameter subject to model calibrations. Most commonly, for calibrating the *DDF*, runoff is used (Hinzman and Kane, 1991; Klok et al., 2001; Luo et al., 2013; Bogacki and Ismail, 2016). However, it is also important to note that the calibration of the *DDF* can be significantly affected by other model parameters due to their interdependency (Gafurov, 2010; He et al., 2014).

Snowmelt runoff modelling using the degree-day approach is very common (Hock, 2003) and popular since air temperature is an excellent surrogate variable for the energy available in near-surface atmosphere that governs the snowmelt process (Lang and Braun, 1990). Despite its simplicity, this approach has proved to be a powerful tool for simulating the complex melt processes especially in large and data scarce catchments (Zhang et al., 2006; Immerzeel et al., 2009; Tahir et al., 2011; Lutz et al., 2016).

Extensive research has been devoted to the enhancement of the original degree-day approach. Braun, (1984) introduced the Temperature-Wind-Index method by inclusion of a wind-dependent scaling factor. A hybrid approach, which combines both, temperature-index and energy balance methods was introduced by Anderson, (1973). Hock, (1999) attempted to improve the simple temperature-index

model by adding a term to consider potential incoming direct solar radiation for clear sky conditions. The potential clear sky solar radiation is calculated as a function of position of the sun, geographic location and a constant atmospheric transmissivity (Hock and Noetzli, 1997; Hock, 1999). This model is comparable with the data requirements of a simple degree-day model. Pellicciotti et al., (2005), considered the net shortwave radiation instead of just incoming shortwave radiation by including snow albedo in their proposed degree-day model. Although all these enhancements focus on adding more physical foundation to the original degree-day method, the classical approach is still more popular because of its simplicity and merely dependence on air temperatures.

A weakness of the degree-day approach is the fact that it works well over longer time periods but with increasing temporal resolution, in particular for sub-daily time-steps, the accuracy decreases (Lang, 1986; Hock, 1999). In addition, the spatial variability of melt rates is not modelled accurately as usually the *DDFs* are considered invariant in space. However, melt rates can be subject to substantial small-scale variations, particularly in high mountain regions due to topography (Hock, 1999). For example, topographic features (e.g. topographic shading, aspect and slope angles) including altitude of a basin can influence the spatial energy conditions for snowmelt and lead to significant variations of the *DDF* (Hock, 2003; Marsh et al., 2012; Bormann et al., 2014). Under otherwise similar conditions, *DDFs* are expected to increase with increasing elevation, with increasing direct solar radiation input and with decreasing albedo (Hock, 2003).

Obviously, the *DDF* cannot be treated as a constant parameter as it varies due to the changes in the physical properties of the snowpack over the snowmelt season (Rango and Martinec, 1995; Prasad and Roy, 2005; Shea et al., 2009; Martinec et al., 2008; Ismail et al., 2015). The spatio-temporal variation in the *DDF* (Zhang et al., 2006; Asaoka and Kominami, 2013) not only affects the accuracy of snow and ice melt modelling (Quick and Pipes, 1977; Braun et al., 1993; Schreider et al., 1997) but also is a key to estimate heterogeneity of the snowmelt regime (Hock, 1999, 2003; DeWalle and Rango, 2008; Braithwaite, 2008; Schmid et al., 2012). Since the melt depends on energy balance processes, changes in *DDFs* are a result of energy components that vary with different climatic conditions (Ambach, 1985; Braithwaite, 1995). Another topic that needs attention is the stationarity of the *DDF* under climate change (Matthews and Hodgkins, 2016). Future water availability under climate change scenarios is typically modelled with *DDFs* calibrated for the present climate, which increases the parametric uncertainty introduced by the hydrological models (Lutz et al., 2016; Ismail and Bogacki, 2018; Hasson et al., 2019; Ismail et al., 2020).

In order to allow for a more process-based estimate of the *DDF*, the present study attempts to quantify the contribution of each energy balance component to melt and subsequently to the overall *DDF*. Considering that degree-day models are typically utilised in large catchments with data scarce conditions, energy balance components are approximated by formulas with minimum data requirement following the approach by Walter et al., (2005). Based on these formulas, the *DDF* contribution corresponding to the respective energy components is quantified in tables and graphs for common

snowmelt conditions, which can be used for a rapid appraisal. The presented approach is open in the

sense that if for any of the energy balance components observed data is available or more sophisticated

110   models are desired, these can easily replace each of the presented approximations.

It shall be emphasised, that the objective of this study is not to incorporate an energy balance based *DDF* approach into temperature index models. The aim is rather to gain a quantitative idea how different factors affect the *DDF* in order to obtain a good estimate and realistic limits for calibration of this model parameter as well as to predict changes during the melt season in case of forecasting or due to the effects

115   of climate change.

2. Study area

The study area covers the Dreisäulerbach catchment, which is a part of Isar River system lies in the sub-alpine region of Bavaria in the Ammergauer Alps. It is approximately located between latitudes 47°34'55"– 47°35'05" North and longitudes 10°56'40"–10°57'07" East. It covers an area of about ~2.3

120   km² and has a mean hypsometric elevation of just over 1200 m a.s.l. (Figure 1). The elevation ranges from about 950 m a.s.l at Linderhof gauging station up to 1768 m a.s.l at the Hennenkopf.

The area is mostly made up by south facing slopes, but also contains northern slopes in southern parts of the catchment (Kopp et al., 2019). The catchment is densely forested which during the winter season is fully snow-covered. The mean annual temperature in the observation period (i.e. November 2016 –

125   May 2021) is about 5.8 °C and the long-term mean annual precipitation at the Ettal-Linderhof station of the Water Science Service Bavaria is reported to be 1676 mm (Kopp et al., 2019).

In order to observe the seasonal snow dynamics, snow measurement instruments in addition to standard meteorological station has been installed at the Brunnenkopfhütte at an elevation of 1602 m a.s.l. (see Figure 2). The installed station has various sensors including temperature, pressure, wind, solar radiation

130   (incoming, outgoing), snow depth, snow scale, snowpack analyzer and pluviometer. Table 1 summarize the observed monthly meteorological data at Brunnenkopfhütte station.

Table 1 Observed monthly average meteorological data – (Brunnenkopfhütte: November 2016 – May 2021)

Variables	Jan	Feb	Mar	Apr	May	Jun	Jul	Aug	Sep	Oct	Nov	Dec
T_a (°C)	-2.48	-0.41	0.52	4.14	6.76	12.40	13.62	14.22	9.69	7.72	3.06	0.08
P [mm]	230.2	147.3	138.8	115.1	188.0	185.4	216.5	241.5	183.7	162.4	107.2	195.9
u (ms⁻¹)	1.08	1.01	1.10	0.97	0.71	0.60	0.59	0.59	0.60	0.79	1.02	1.00
RH (%)	74.2	69.3	73.4	72.2	82.1	78.2	76.7	78.1	82.8	71.7	70.5	69.4
*A (-)	0.80	0.74	0.69	0.51	0.42	-	-	-	-	-	0.45	0.72
K_T (-)	0.51	0.52	0.53	0.53	0.40	0.43	0.43	0.45	0.48	0.55	0.50	0.49
SR_{in} (KJ m⁻²d⁻¹)	5310	8367	12814	17270	15628	17922	17320	15997	12989	10282	5899	4408

* Albedo (A): only considered when ground is snow covered.

135
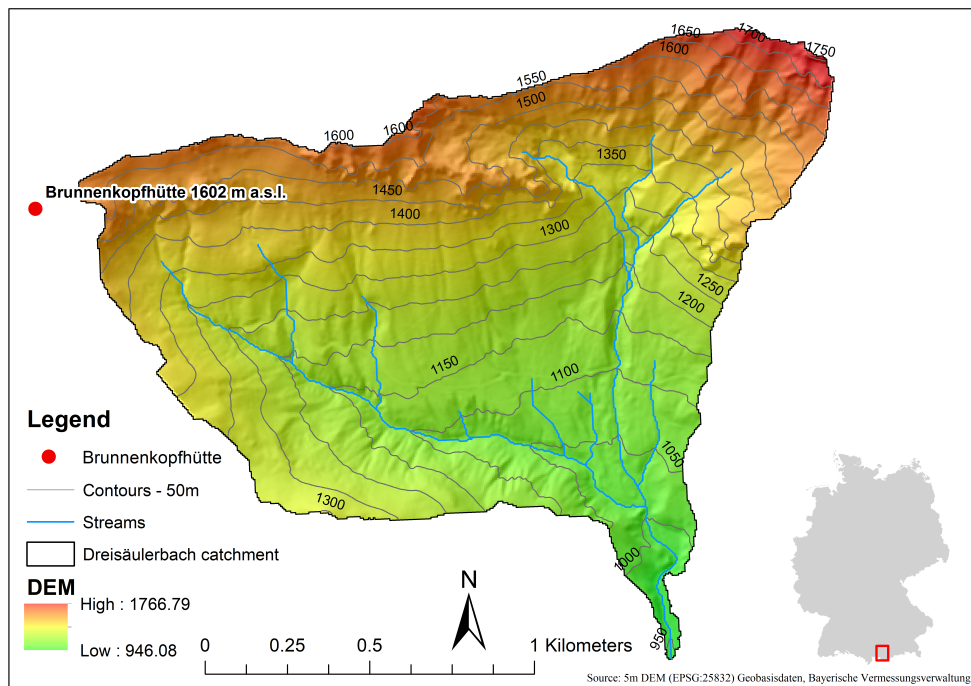
Figure 1 Location of Brunnenkopfhütte snow station in the Dreisäulerbach catchment – German Alps

140   **Figure 2** Automatic weather and snow measurement station at Brunnenkopfhütte in Ammergauer Alps [1602 m a.s.l.] (Image credit – Wolfgang Bogacki, 2016)

3. Materials and methods

145 The primary objective of this paper is to analyze the contribution of individual energy balance components to snowmelt, in order to better understand and probably to predict, how the lumped degree-day factor will vary with the season, latitude, altitude, and the concrete meteorological conditions. In addition, we want to demonstrate along the approach of Walter et al., (2005), how these energy balance components can be estimated with minimal data requirements, as limited data availability is the major reason to apply temperature-index respectively degree-day factor models.

150 ### 3.1 Degree-Day Factor

The basic formulation of the degree-day method to calculate daily snowmelt depth M (mm) multiplies the number of degree-days T_{DD} (°C d) with the degree-day factor DDF (mm °C^{-1} d^{-1}) (Rango and Martinec, 1995).

$$M = DDF \times T_{DD} \qquad (1)$$

Degree-days T_{DD} are only defined if a characteristic air temperature lies above a reference temperature;
155 otherwise, T is set to 0°C. Typically, the freezing point 0°C is chosen as reference temperature. The characteristic air temperature is usually calculated by the average of daily minimum and maximum temperature, but other approaches like the mean of hourly temperature observations, daily maximum temperature (Bagchi, 1983), or integrating only the positive temperatures of a day (Rango and Martinec, 1995; Ismail et al., 2015) are also common. By a simple re-arrangement of eq. (1) to

$$DDF = \frac{M}{T_{DD}} \qquad (2)$$

160 the DDF can be back-calculated for given degree-days T_{DD}, if the daily melt depth M is known either by observation or by calculation. Likewise, the portion of the degree-day factor DDF$_i$ associated to the melt depth M_i related to any of the individual energy balance components (see eq. (4)) can be determined.

The energy needed to melt ice at 0°C into liquid water at 0°C is defined by the latent heat of fusion of ice (333.55 kJ kg^{-1}). Thus the melt depth M_i caused by an energy flux Q_i (W m^{-2}) over a certain time-
165 period Δt (s) can be calculated from the relation (USACE, 1998; Hock, 2005)

$$M_i = \frac{Q_i}{\lambda \, \rho_w} \Delta t \cong 3.00 \times 10^{-6} \, Q_i \Delta t \qquad (3)$$

where ρ_w is the density of water at 0°C (999.84 kg m^{-3}). In the context of degree-day factor models, the time-period Δt is usually taken as 1 day = 86400 s, though some authors (Hock, 1999; McGinn, 2012) have calculated degree-day factors also for sub-daily, e.g. hourly periods. According to the relation given in eq. (3), an energy flux of 1 W m^{-2} for 1 day will result in a melt depth of 0.26 mm.

3.2 Energy Balance

The energy flux available for snowmelt Q_M can be calculated from the balance of energy fluxes over the surface of the snowpack and the change in the internal energy stored in the snowpack ΔQ (e.g. USACE, 1998)

$$Q_M = Q_S + Q_L + Q_H + Q_E + Q_G + Q_P - \Delta Q \qquad (4)$$

where Q_S and Q_L are the net short- and longwave radiation, Q_H is the sensible heat, Q_E the latent energy of condensation or vaporization, Q_G the heat conduction from the ground, and Q_P the energy contained in precipitation (all terms in W m^{-2}).

In the following sections, the individual components of the energy balance will be discussed in more detail.

3.2.1 Shortwave Radiation

Shortwave radiation emitted from the sun is usually the most important source of energy input to the snowpack. The net energy flux Q_S (W m^{-2}) entering the snowpack by absorption of shortwave radiation is (USACE, 1998)

$$Q_s = (1 - A)S_i \qquad (5)$$

where A is the snow albedo (–) and S_i the incident solar radiation (W m^{-2}) on the snow surface. A widely used approach to determine the incident solar radiation on earth's surface is the introduction of a clearness index K_T (–)

$$S_i = K_T S_0 \qquad (6)$$

where S_0 is the mean daily potential extra-terrestrial solar radiation (W m^{-2}) that would insolate a horizontal surface on the earth's ground if no atmosphere would be present. The potential insolation, which is only dependent on the changing position of the sun during the year in relation to the geographic location of the incident point on the earth's surface, can be calculated from the equation (Masters, 2004)

$$S_0 = G_s \frac{1}{d_r{}^2} \frac{1}{\pi} (\cos(\emptyset)\cos(\delta)\cos(\omega_s) + \omega_s \sin(\emptyset)\sin(\delta)) \qquad (7)$$

where G_S is the solar constant (W m^{-2}), d_r the relative distance earth to sun (–), ϕ the geographic latitude (rad) of the incident point, δ the solar declination (rad), and ω_s the sunrise hour angle (rad). The solar constant G_S is slightly varying with the occurrence of so-called sunspots, however a constant value of 1367 W m^{-2} has been used for the last decades. New measurements indicate a somewhat lower value of 1361 W m^{-2} (Kopp and Lean, 2011).

195 Both sun position variables, the relative distance earth to sun and the solar declination, can be calculated quite exactly by rigid astronomical algorithms (Meeus, 1991; Reda and Andreas, 2004) however for non-astronomical purposes, more simple formulas are sufficiently accurate. The relative distance earth to sun, which is varying over the year due to the elliptical orbit of the earth, can be approximated by (Masters, 2004)

$$\frac{1}{d_r{}^2} \approx 1 + 0.034 \cos\left(\frac{2\pi.J}{365}\right) \qquad (8)$$

200 where J is the day of the year, while the solar declination can be obtained from the sinusoidal relationship

$$\delta \approx 0.409 \sin\left(\frac{2\pi}{365}(J - 81)\right) \qquad (9)$$

that puts the spring equinox on day $J = 81$. Knowing the solar declination δ, the sunrise hour angle ω_s can be calculated from

$$\cos\omega_s = -\tan(\emptyset)\tan(\delta) \qquad (10)$$

On the northern hemisphere the maximum extra-terrestrial radiation occurs at the summer solstice with a fairly identical mean daily energy flux of about 480 W m^{-2} over latitudes $30° - 60°$ North, as the sun's
205 lower altitude angle at higher latitudes is compensated by longer daylight hours. On the contrary, minimum extra-terrestrial radiation at the winter solstice varies strongly with latitude, e.g. 227 W m^{-2} at $30°$ and only 24 W m^{-2} at $60°$ North.

When the solar radiation passes through the atmosphere, it is partly scattered and absorbed. While even on a clear day only about 75% of the incoming radiation reaches the ground, by far the largest attenuation
210 is caused by clouds. A vast number of solar radiation models exist that parameterize this effect, which is denoted as clearness index K_T or atmospheric transmissivity τ, as a function of meteorological variables. For a review see e.g. Evrendilek and Ertekin (2008), Ahmad and Tiwari (2011), or Ekici (2019).

A fundamental and widely used solar radiation model which is proposed in the context of
215 evapotranspiration calculations (Allen et al., 1998) is the Ångström-Prescott model, that relates the clearness index to the relative sunshine duration

$$K_T = \frac{S_i}{S_0} = a + b\frac{n}{N} \qquad (11)$$

with n is the actual and N the maximal possible duration of sunshine (hr) where the latter can be calculated from the sunrise hour angle ω_s by

$$N = \frac{24}{\pi}\omega_s \tag{12}$$

The parameters a and b in eq. (11) are regression parameters, that usually have to be fitted to observed
220 global radiation. In case no actual solar radiation data is available, the values $a = 0.25$ and $b = 0.50$ are
recommended (Allen et al., 1998). Though the Ångström-Prescott model has the disadvantage, that the
parameters have to be fitted and the actual duration of sunshine has to be observed, it has the benefit,
that both parameters allow for a direct physical interpretation and a straight demonstration of the effects
of cloud cover. The parameter a represents the clearness index K_T on overcast days ($n = 0$), while their
225 sum $a + b$ gives the clearness index on clear days ($n = N$).

In the common situation in remote mountainous regions, that only temperature data is available, another
group of solar radiation models can be utilised, which uses the difference between daily maximum and
minimum air temperature ΔT (°C) as a proxy for cloud cover, because clear sky conditions result in a
higher temperature amplitude between day and night than under overcast conditions. Typical models
230 are the exponential approach proposed by Bristow and Campbell (1984) and its later modifications or
the simple empirical equation by Hargreaves and Samani (1982)

$$K_T = k.\sqrt{\Delta T} \tag{13}$$

with the empirical coefficient $k = 0.16$ for inland and $k = 0.19$ for coastal locations.

It is obvious, that the attenuation of extra-terrestrial solar radiation is a function of the distance the rays
have to travel through the atmosphere, as absorption and scattering occurs all along the way. Several
235 solar radiation models consider altitude as a variable, from which the models below are of Ångström-
Prescott type, thus the altitude effects can be directly compared.

Jin et al. (2005):

(a)
$$K_T = (0.0855 + 0.0020\emptyset + 0.030z) + 0.5654\frac{n}{N} \tag{14}$$

(b)
$$K_T = (0.1094 + 0.0014\emptyset + 0.0212z) + (0.5176 + 0.0012\emptyset + 0.0150z)\frac{n}{N} \tag{15}$$

Rensheng et al. (2006):

$$K_T = (0.122 + 0.001\emptyset + 0.0257z) + 0.543\frac{n}{N} \tag{16}$$

Liu et al. (2019):

$$K_T = (0.1755 + 0.0136z) + (0.5414 + 0.0117z)\frac{n}{N} \tag{17}$$

240   For all models, z is the altitude (km) and ϕ the latitude (deg). In order to separate the altitude effect from other parameters, a clearness altitude factor K_Z (–) with

$$K_z = \frac{K_T}{K_{T_0}} \tag{18}$$

is introduced, where K_{T_0} is the clearness factor at $z = 0$ m a.s.l. which results in $K_Z = 1$ at sea level for all models and all values of relative sunshine duration n/N. Though the individual clearness altitude factors obtained from the above models are different, they all exhibit a constant increase per unit altitude

245   for a given n/N and highest values for overcast conditions ($n/N = 0$) while the altitude effect under clear sky conditions ($n/N = 1$) is significantly smaller.

While the albedo of fresh snow is well above 0.9 (Hock, 2005), indicating that most of the shortwave radiation is reflected, it may drop significantly within a few days due to snow metamorphism. Well aged snow generally has an albedo in the range of $0.4 - 0.5$ (Anderson, 2006). Snow albedo is primarily

250   dependent on the grain size of the snow crystals near the surface but also on aerosols in the snow and dust deposits. Respective snow albedo models are proposed e.g. by Wiscombe and Warren (1980) and Warren and Wiscombe (1980) however, due to the data requirements, commonly surrogate exponential decay models as formulated by (USACE, 1956) are used, which assume the decrease of albedo as a function of time after the last significant snowfall. For example Walter et al., (2005) use the empirical

255   relationship

$$A_n = 0.35 - (0.35 - A_{max}).\,exp\left[-\left(0.177 + \ln\left(\frac{A_{max} - 0.35}{A_{n-1} - 0.35}\right)^{2.16}\right)\right]^{0.46} \tag{19}$$

where, A_{n-1} is the albedo of the previous day and A_{max} is the maximum albedo (~0.95) of fresh snow. Following eq. (19), the snow albedo will decrease from 0.95 to 0.52 after 10 days and to 0.43 after 30 days if no new snowfall occurs.

3.2.2   Longwave Radiation

260   The longwave radiation net energy flux over the snow surface Q_L (W m^{-2}) is the balance

$$Q_L = Q_{L,in} - Q_{L,out} \tag{20}$$

between incoming longwave radiation that is emitted by the atmosphere $Q_{L,in}$ (W m^{-2}) and outgoing radiation from the snowpack $Q_{L,out}$ (W m^{-2}).

Longwave radiation is a function of the temperature of the emitting body and can be calculated with the Stefan-Boltzmann law

$$L = \varepsilon\,\sigma\,T^4 \tag{21}$$

265   where L is the radiative flux (W m^{-2}), ε and T are the emissivity (–) and the absolute temperature (K) of the emitting body, and σ is the Stefan-Boltzmann constant (5.67×10^{-8} W m^{-2} K^{-4}).

In particular fresh snow is nearly a perfect blackbody with respect to longwave radiation, thus it has a high emissivity of 0.99 (Warren, 1982; USACE, 1998; Anderson, 2006). For old snow, Brutsaert (1982) gives an emissivity value of 0.97. Given a melting snowpack having a surface temperature of 0°C, the

270   outgoing energy flux can be taken as constant with $Q_{L,out} \sim 310$ W m^{-2}.

For the atmospheric longwave radiation, usually the air temperature T_a (K) is used in eq. (21). However, while the snowpack longwave emissivity is virtually a constant, the emissivity of the atmosphere is highly variable. Typical values under clear sky conditions range from 0.6 – 0.8, primarily depending on air temperature and humidity (Anderson, 2006) whereas for overcast conditions it can be close to 1.0.

275   A number of empirical and more physically based approaches exist to estimate atmospheric longwave emissivity from standard meteorological data (see Hock, 2005 for a discussion). For clear sky conditions, Brutsaert (1975) developed a theoretically based formula depending on air temperature and vapour pressure

$$\varepsilon_{ac} = 1.24 \left(\frac{p_v}{T_a}\right)^{\frac{1}{7}} \qquad (22)$$

where ε_{ac} is the clear sky longwave emissivity (–), p_v the actual vapour pressure (hPa), and T_a the air

280   temperature (K). Later, Brutsaert reconciled eq. (22) with an empirical approach proposed by Swinbank (cited in Brutsaert, 1982)

$$\varepsilon_{ac} = 9.2 \times 10^{-6} \, T_a^2 \qquad (23)$$

that considers the strong correlation between vapour pressure and air temperature, thus only air temperature is needed as input variable. Using above relation, at an air temperature of 10 °C the atmospheric longwave radiation flux into the snowpack will amount to $Q_{L,in} = 281$ W m^{-2} under clear

285   sky conditions, which is less than the outgoing flux of 310 W m^{-2}, i.e. the snowpack will lose energy in this situation.

The variability of atmospheric emissivity due to cloud cover, which increases the longwave emissivity, is significantly higher than variations under clear sky conditions. Monteith and Unsworth (2013) give the simple linear relationship.

$$\varepsilon_a = (1 - 0.84c)\varepsilon_{ac} + 0.84c \qquad (24)$$

290   where ε_a is the atmospheric longwave emissivity, c the fraction of cloud cover (–), and ε_{ac} is calculated by eq. (22) or eq. (23). For overcast conditions and an air temperature of 10 °C, eq. (24) yields an atmospheric emissivity of 0.96, which results in an atmospheric longwave radiation flux of $Q_{L,in} = 351$ W m^{-2} and thus a positive flux of $Q_L = 41$ W m^{-2} into the snowpack.

Although cloud cover is difficult to parameterise as clouds can be highly variable in space and time and
effects on radiation dependent on the different cloud genera, a strong correlation between cloud cover
and sunshine duration is obvious. Doorenbos and Pruitt, (1977) give a tabulated relation between
cloudiness c and relative sunshine hours n/N (see eq. 11), that can be fitted by the quadratic regression

$$c = 1 - 0.5544 \frac{n}{N} - 0.5483 \left(\frac{n}{N}\right)^2 \qquad (25)$$

Nevertheless, in simple sky models usually a linear relation between cloudiness and relative sunshine
hours is applied as a first approximation (e.g. Brutsaert, 1982; Annandale et al., 2002; Pelkowski, 2009),
for which Badescu and Paulescu, (2011) give a probabilistic reasoning.

3.2.3 Sensible Heat Exchange

Sensible heat exchange describes the energy flux due to temperature differences between the air and the
snow surface while air is permanently exchanged by wind turbulences. A frequent approach to
parameterise turbulent heat transfer is the aerodynamic method, that explicitly includes wind speed as a
variable (Braithwaite et al., 1998; Lehning et al., 2002; Hock, 2005).

$$Q_H = \rho_a c_p C_H u (T_a - T_s) \qquad (26)$$

where ρ_a is the air density (~1.29 kg m^{-3}), c_p the specific (isobaric) heat capacity of air (= 1006 J kg^{-1} °C^{-1}), C_H the exchange coefficient for sensible heat (–), u the mean wind speed (m s^{-1}), T_a the air temperature
(°C), and T_s the temperature at the snow surface (°C).

The exchange coefficient C_H can be approximated with (Campbell and Norman, 1998)

$$C_H = \frac{k^2}{ln\left(\frac{z_u}{z_m}\right) ln\left(\frac{z_T}{z_h}\right)} \qquad (27)$$

where k is the von Karman's constant 0.41 (–), z_u and z_T the height of wind and temperature observation
above the snow surface (m), z_m the momentum roughness parameter, and z_h the heat roughness
parameter. For a snow surface, the roughness parameters are given by Walter et al., (2005) as z_m
~ 0.001 m and z_h ~ 0.0002 m.

Eq. (27) is equivalent to the calculation of aerodynamic resistance in the Penman-Monteith equation
(Allen et al., 1998) when applying a zero plane displacement for the snow surface and assumes neutral
stability conditions, i.e. temperature, atmospheric pressure, and wind velocity distributions follow nearly
adiabatic conditions. Otherwise, diabatic correction factors (see Campbell and Norman, 1998) have to
be applied.

As can be seen from eq. (26), the sensible heat component is mainly dependent on wind speed and air
temperature. During stable clear weather periods with typically light winds, the turbulent exchange is of

less importance compared to the radiation components. For example, a wind speed of 1 m s^{-1} and an air temperature of 5 °C will result in a sensible heat flux of about 17 W m^{-2}. However, at warm rain events or at Föhn conditions with strong warm winds, turbulent exchange can significantly contribute to the melt process.

3.2.4 Latent Energy of Condensation or Vapourisation

325

The latent energy exchange reflects the phase change of water vapour at the snow surface, either by condensation of vapour contained in the air or by vapourisation of snow. Thus, it can either warm or cool the snowpack (Harpold and Brooks, 2018). The energy flux is dependent on the vapour gradient between air and snow surface and is, like the sensible heat exchange, a turbulent process that increases

330 with the wind speed. Thus, the aerodynamic formulation is analogously to eq. (26)

$$Q_E = \rho_a \lambda_v C_E u(q_a - q_s) \tag{28}$$

where λ_v is the latent heat of vapourisation of water at 0°C (= 2.501×10⁶ J kg^{-1}), C_E the exchange coefficient for latent heat (–) which is assumed to be equal to the exchange coefficient for sensible heat C_H, q_a the specific humidity of the air (–), and q_s the specific humidity at the snow surface (–).

The specific humidity q_a can be derived from measurements of relative humidity or dew point

335 temperature. In cases where such data is not available, Walter et al., (2005) approximate the dew point temperature by the minimum daily temperature. For any air temperature T (°C), the saturation vapour pressure p_0 (Pa) can be calculated by an empirical expression known as the Magnus-Tetens equation in the general form (Lawrence, 2005)

$$p_0 = C \, e^{\frac{A \, T}{B+T}} \tag{29}$$

where A, B, and C are coefficients e.g. after Allen et al., (1998) A = 17.2694, B = 237.3 °C, C = 610.78

340 Pa. At the snow surface, according to Lehning et al., (2002) the air temperature can be assumed equal to the snow surface temperature and eq. (29) is applied with coefficients for saturation vapour pressure over ice A = 21.8746, B = 265.5 °C, C = 610.78 Pa (Murray, 1967). At a temperature of 0°C, both coefficient sets yield the same saturation vapour pressure of p_0 = 611 Pa.

Knowing the vapour pressure p_v (Pa) at a given temperature, the respective specific humidity of the air

345 or at the snow surface can be calculated by

$$q = \frac{e \, p_v}{p - (1-e)p_v} \approx \frac{e}{p} p_v \tag{30}$$

where p is the atmospheric pressure (Pa) and e the ratio of molar weights of water and dry air = 0.622. Thus, similar to the sensible heat flux Q_H, the latent energy exchange at the snow surface Q_E can be taken as a function of wind speed in combination with air and snow surface temperature, where the latter is assumed as 0°C at melting conditions.

350   While at positive air temperatures the sensible heat flux is always warming the snowpack, the latent heat flux can cool the snow by vapourisation if the relative humidity of the air is low. Even when assuming a relative humidity of 100% the latent heat flux into the snowpack will be comparatively small if wind speed is low, e.g. about 13 W m^{-2} at an air temperature of 5 °C and a wind speed of 1 m s^{-1}.

3.2.5   Ground Heat

355   Heat conduction from the ground into the snowpack is small and can be in general neglected except when first snow falls on warm ground (Anderson, 2006). If the snowpack is well established, due to the low thermal conductivity of snow the heat flux across the soil-snow interface becomes independent of air temperature fluctuations and depends only on the thermal conductivity of the soil and the temperature gradient in the upper soil layer. USACE, (1998) gives a range between 0 – 5 W m^{-2} for constant daily
360   values. DeWalle and Rango, (2008) approximate a flux of 4 W m^{-2} assuming a soil temperature of 1 °C at a depth of 0.5 m, and a soil thermal conductivity of 2 W m^{-1} °C^{-1} that is at the higher end of the range of 0.2 – 2 W m^{-1} °C^{-1} given by Oke, (1987). It has to be noted, that the soil temperature gradually approaches the snowpack temperature during the winter (USACE, 1956; Marks et al., 1992), thus ground heat conduction will generally decrease. Own measurements of soil temperature show a similar
365   behaviour. Soil temperature dropped from 1 – 3 °C shortly after establishment of the snowpack to > 0 – 1 °C after about a month and then stayed constant until final melt.

3.2.6   Precipitation Heat

The heat transfer into the snowpack by lowering rain's temperature, that is usually assumed to be equal to the air temperature T_a (°C), down to the freezing point at 0°C can be estimated as

$$Q_P = c_w\, P\, T_a \tag{31}$$

370   where c_w is the specific heat capacity of water (4.2 kJ kg^{-1} °C^{-1}) and P is the daily rainfall depth (kg m^{-2} d^{-1}). The energy input from precipitation is usually quite small and even extreme weather situations, like heavy warm rain storms with temperatures of 15°C and a precipitation depth of 50 mm, that may occur e.g. during early winter in the alps, would result in a modest mean daily energy flux of 36.5 W m^{-2} where it has to be taken into account, that such events are only singular.

3.2.7   Change in Internal Energy

375   The rate of change in the energy stored in the snowpack ΔQ (W m^{-2}) represents the internal energy gains and losses due to the change of snow temperature and the melting of the ice portion or refreezing of liquid water in the snow. Until the snowpack temperature is isothermal at 0°C, any melt produced by surplus energy in the surface layer of the snowpack will percolate downward when the liquid water holding capacity of the porous snow matrix is exceeded and may be refrozen in colder lower layers. If
380   a snowpack is isothermal at 0°C and is saturated, i.e. the residual volumetric water content of about 8% (Lehning et al., 2002) is filled with liquid water, the snowpack is called 'ripe'. In that state, any additional energy input will immediately produce snowmelt runoff according to eq. (3). If however a

snowpack is still in the ripening phase, at least part of the incoming energy is absorbed to decrease the
385   energy deficit and has to be subtracted from energy available for melt thus will reduce the respective
DDF. The energy needed to bring the snowpack temperature isothermal at 0°C, i.e. the snowpack's
energy deficit, is usually expressed as 'cold content' (Marks et al., 1999; Schaefli and Huss, 2011;
Jennings et al., 2018).

The present paper aims to demonstrate the contribution of each energy flux component towards a
390   resulting *DDF*. In this respect, the energy deficit in the ripening phase plays no role, as each flux
component is analysed individually. Only when it comes to a comparison with observed melt data (see
Sec. 4.6) the ripening state of the snowpack has to be taken into account. In this context, the study
focusses only on melt periods where the snowpack is ripe while melt periods where the cold content is
increased e.g. by new snow events or significant cooling phases are excluded from the analysis.

395   Certainly it is of interest to estimate *DDFs* also in cases where an internal energy deficit exists, e.g.
because of radiational cooling during clear cold nights. The cold content usually is either estimated as a
function of meteorological parameters or calculated by keeping track of the residuals of the snowpack
energy balance (Jennings et al., 2018). The SNOWPACK model (Lehning et al., 2002), that is
operationally employed on a day-to-day basis for avalanche warning, is an excellent tool for a detailed
400   simulation of the vertical mass, energy, and besides other state variables the snow temperature
distribution inside a snowpack, taking into account the complex processes of snow metamorphosis and
heterogeneity of layers in the snowpack, and as a by-product, also simulates snowmelt runoff. However,
SNOWPACK requires a considerable number of qualified input variables with preferably at least hourly
observations, which both is usually not available in the context where degree-day factor models are
405   employed.

On the other hand Walter et al., (2005) apply a lumped approach, that accounts for the cold content by
changing the (isothermal) snowpack temperature depending on the daily net energy flux. When the
incoming energy flux is sufficient to raise the snow temperature to 0°C or when it is already at 0°C the
day before, all additional available energy produces melt. This appealing approach, which does not need
410   any additional data, however seems to significantly over-estimate the snowpack temperature in
particular in situations with negative energy fluxes at night but a positive daily net balance, as a
comparison with SNOWPACK results and with observations at Brunnenkopfhütte shows. Thus a
suitable parametrisation of the cold content, that would enable satisfactory estimates of *DDFs* in
situations when the snowpack is not completely ripe, remains subject to further research.

415   **4. Results**

In this section, the contribution of each energy flux component Q_i to the lumped daily *DDF* is presented.
For this purpose, the respective melt depth M_i is calculated according to eq. (3) and further converted
into the corresponding degree-day factor component DDF_i using eq. (2). Degree-days T_{DD} (°C d) in eq.

(2) are estimated by the average daily air temperature, thus having the same numerical value as the air
temperature T_a (°C) used in the calculation of several energy flux components.

Besides demonstrating the dependency of the *DDF* components on decisive parameters of the energy
flux components, the presented tables and graphs, which are based on the approximate relationships
given in section 3, can be used to estimate the *DDF* component values in case either observed data is
not available or not sufficient for more sophisticated approaches. It should be noted that parameters are
normalised where applicable, i.e. set to hypothetical values like clearness index $K_T = 1$ or wind speed u
$=1.0$ m s^{-1}, thus final *DDF* values can be obtained by multiplying the given figures by the actual values
of those parameters. Furthermore, all results are based on the assumption that the snowpack is isothermal
at 0°C and in fully ripe state.

4.1 Shortwave radiation component - DDF$_S$

Shortwave radiation induced melt is usually considered the most important *DDF* component especially
at higher altitudes. The net energy flux Q_S is calculated using eq. (5), which consists of three factors (a)
latitude, (b) albedo, and (c) clearness index K_T. The dependency of DDF$_S$ on these factors is
demonstrated in Figure 3 for the period between winter solstice (21st December) and summer solstice
(21st June). As shortwave radiation is independent of air temperature and hence of degree-days, the
corresponding melt is divided by a hypothetical degree-day value of 1 °C d to arrive at DDF$_S$ values as
presented. In case of actually higher degree-days, the given DDF$_S$ values have to be divided accordingly.

Figure 3 (a) shows the variation of DDF$_S$ depending on latitude for the range 30° – 60° North, while
albedo ($A = 0$) and clearness index ($K_T = 1$) are set constant. Obviously, there is a significant difference
in DDF$_S$ for different latitudes around the winter solstice due to solar inclination, making latitude the
predominant factor for DDF$_S$ at this time of the year. However, around the summer solstice, DDF$_S$ has
nearly the same value at different latitudes because the lower solar angle at higher latitudes is
counterweighted by a larger hour angle, i.e. longer sunlight hours. Thus, with the progress of the melting
season the factors albedo and clearness index become more important than latitude.

Figure 3 (b) shows the influence of albedo on the DDF$_S$ at a given latitude (Brunnenkopfhütte station
latitude 47.58°) and normalised constant clearness index ($K_T = 1$). Snow albedo is varied between 0.9 –
0.4 covering the range between fresh and well-aged snow. As to be expected, the influence of albedo
increases with increasing incoming solar radiation towards the summer solstice. A good estimate of
albedo is therefore much more important when the snowmelt season progresses than in early spring. If
for example the same degree-day value of 10 °C d is assumed on 21st March and on 21st May, the
difference in DDF$_S$ between fresh ($A = 0.9$) and aged ($A = 0.4$) snow would be 0.8 and 4.6 mm °C^{-1} d^{-1}
in March compared to 1.2 and 7.1 mm °C^{-1} d^{-1} in May respectively.

The dependency of DDF$_S$ on the clearness index K_T is shown in Figure 3 (c). As also evident from eq.
(6), DDF$_S$ under clear sky ($K_T = 0.75$) is always higher than under overcast conditions ($K_T = 0.25$).

Similar to albedo, the influence of the clearness index becomes more pronounced, and thus the
455   assessment of clearness conditions more important, with increasing solar angle when the snowmelt
season progresses.

The influence of altitude on DDF_S in terms of increasing K_T values can be considered separately by
multiplying K_{T_0} (at $z = 0$ m a.s.l.) calculated by any of the numerous solar radiation models with a
clearness altitude factor as given in eq. (18). Figure 4 shows the range of clearness altitude factors for
460   latitude 45° derived from four solar radiation models, which were calibrated including high altitude data
(see Sec. 3.2.1). The dark grey area indicates the common overlap of the four models. All of these
models show the same tendency of linear increase by altitude, with the altitude factor being
comparatively smaller under clear sky compared to overcast conditions. When averaging models as well
as sky conditions, the clearness altitude factor and thus the resulting DDF_S increases by about 6% for
465   each 1000 m altitude.
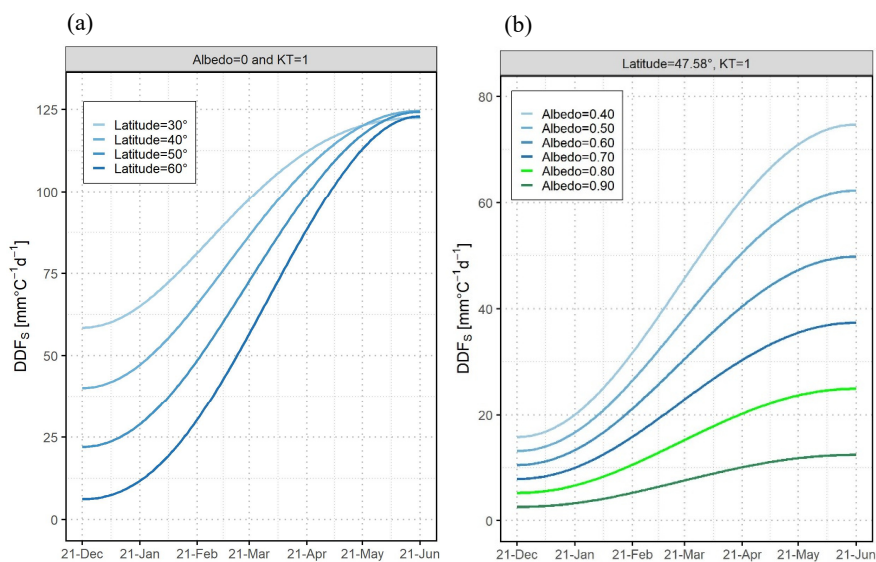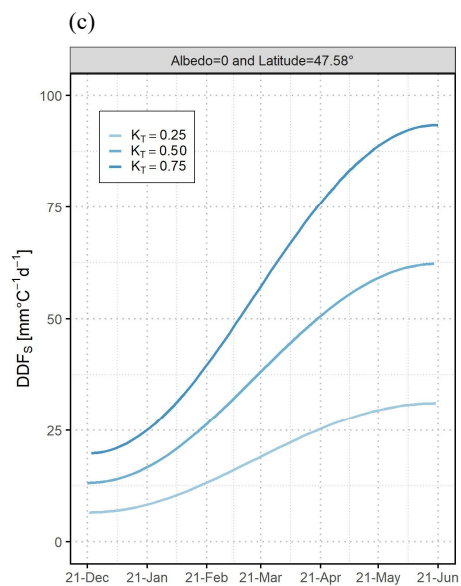
Figure 3 Variation of solar radiation based DDF_S for a degree-day value of 1°C d (a) for different latitudes under constant snow albedo and clearness index (b) for different snow albedo under constant latitude and clearness index (c) for different clearness index under constant latitude and snow albedo – Latitude 47.58° corresponds to the location of Brunnenkopfhütte snow station

470
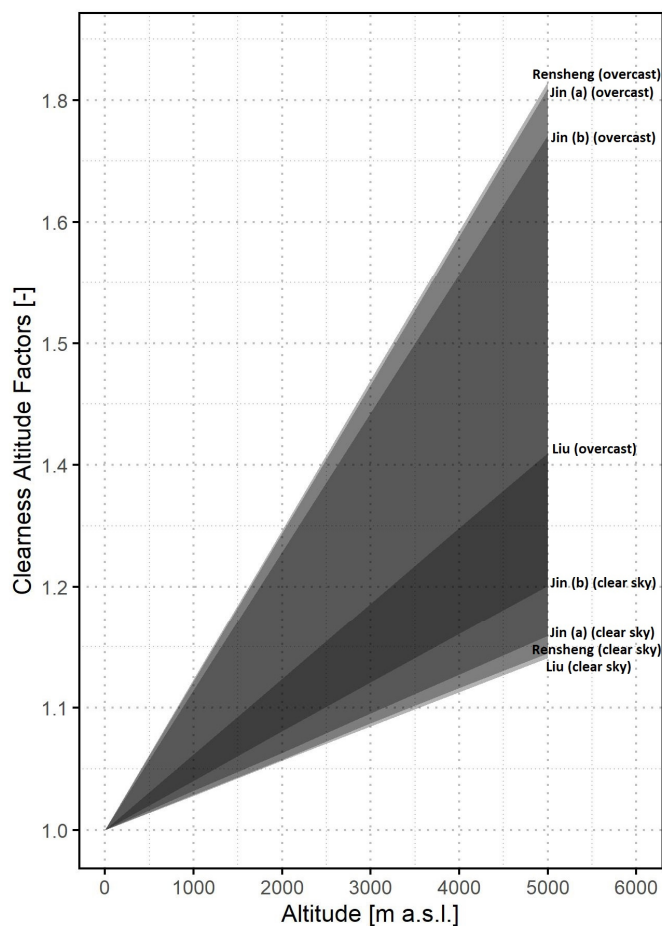
475

Figure 4 Clearness altitude factor for different altitudes ranges, based on different models presented in equations (14 – 17, i.e. Jin (a), Jin (b), Rensheng, and Liu) for latitude 45° where applicable

4.2 Longwave radiation component - DDF_L

The net longwave energy flux Q_L is calculated using eq. (20), in which the outgoing radiation from the

480   snowpack can be assumed as constant. Thus, the contribution of longwave radiation component DDF_L is mainly dependent on air temperature and the emissivity of the atmosphere, in particular cloudiness conditions. Figure 5 and Table 2 present the DDF_L as a function of degree-days T_{DD}, which are equivalent to the average daily air temperature, and cloudiness. For a wide range of degree-days especially in conjunction with low cloudiness, the outgoing longwave energy flux is higher than the

485   incoming, resulting in a theoretically negative degree-day factor that will reduce the total DDF. This means that the DDF_L component under clear sky conditions usually is rather contributing to a cooling of the snowpack than to melting. Under overcast conditions, the DDF_L is relatively constant around 1

mm °C^{-1} d^{-1} with a maximum value of 1.3 mm °C^{-1} d^{-1} at T_{DD} = 20 °C d. Although this contribution to the total *DDF* is small compared to the shortwave radiation component DDF$_S$, it can be of importance

490   at the onset of snowmelt in early spring, when the solar radiation is still low and the albedo of fresh snow is high.

Table 2 Longwave radiation component (DDF$_L$) [mm °C^{-1} d^{-1}] for selected cloudiness [%]

T_{DD} [°C d]	DDF$_L$ Cloudiness										
	0%	10%	20%	30%	40%	50%	60%	70%	80%	90%	100%
1	-19.08	-17.17	-15.26	-13.35	-11.45	-9.54	-7.63	-5.72	-3.81	-1.90	0.01
2	-8.89	-7.94	-6.99	-6.04	-5.09	-4.14	-3.19	-2.24	-1.29	-0.33	0.62
3	-5.49	-4.86	-4.23	-3.59	-2.96	-2.33	-1.70	-1.07	-0.44	0.19	0.82
4	-3.78	-3.31	-2.84	-2.37	-1.90	-1.42	-0.95	-0.48	-0.01	0.46	0.93
5	-2.75	-2.38	-2.00	-1.63	-1.25	-0.88	-0.50	-0.13	0.25	0.62	1.00
6	-2.06	-1.75	-1.44	-1.13	-0.82	-0.51	-0.20	0.11	0.43	0.74	1.05
7	-1.57	-1.30	-1.04	-0.77	-0.51	-0.24	0.02	0.29	0.55	0.82	1.08
8	-1.19	-0.96	-0.73	-0.50	-0.27	-0.04	0.19	0.42	0.65	0.88	1.11
9	-0.90	-0.69	-0.49	-0.29	-0.08	0.12	0.32	0.53	0.73	0.93	1.14
10	-0.66	-0.48	-0.30	-0.11	0.07	0.25	0.43	0.61	0.79	0.98	1.16
15	0.08	0.19	0.31	0.43	0.54	0.66	0.77	0.89	1.01	1.12	1.24
20	0.48	0.56	0.64	0.72	0.81	0.89	0.97	1.05	1.13	1.21	1.30
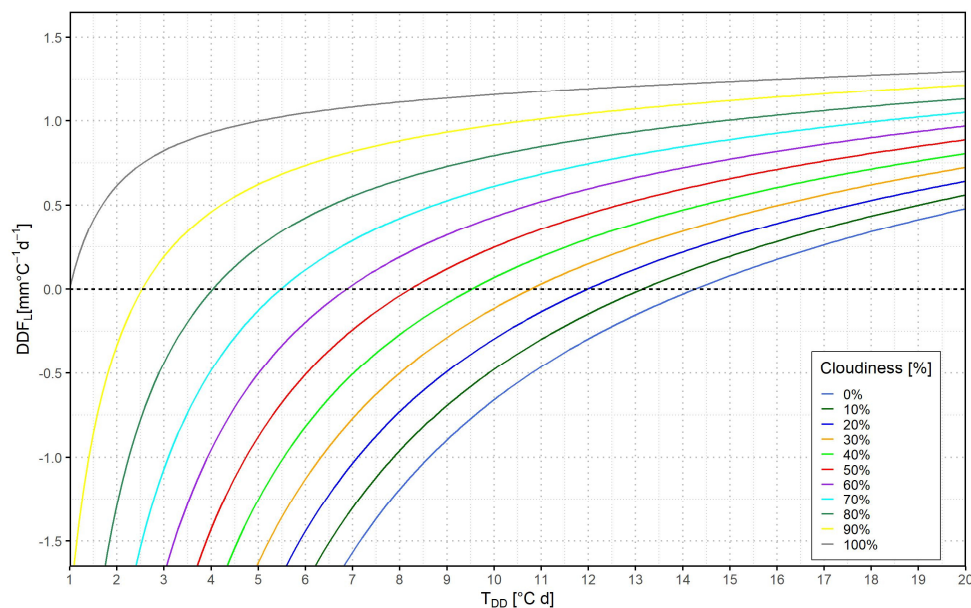
Figure 5 Longwave Radiation component (DDF$_L$) for selected cloudiness [%]

4.3 Sensible heat component - DDF_H

The sensible heat flux Q_H as given by eq. (26) is linear dependent on the temperature difference between air and snow surface. If the snowpack temperature is assumed to be constant at $T_s = 0$ °C, the division by degree-days according to eq. (2) makes DDF_H independent of temperature and proportional to the wind speed, resulting in a value of 0.86 mm °C^{-1} d^{-1} for an average daily wind speed of $u = 1.0$ m s^{-1}. DDF_H for any other wind speed can easily be obtained by multiplication with the actual average daily value. Table 3 presents some examples for different values of u. It should be noted that Table 3 refers to melt conditions with positive air temperature, whereas negative air temperature would lead to respective negative DDF_H resulting in a cooling of the snowpack and a decrease of total DDF.

If wind speed observations are not available, DDF_H may be approximated using typical values. Stigter et al., (2021) for example give a range of wind speed at two different sites in the central Himalayas. At Ganja La the wind speed is generally low i.e. < 2 m s^{-1} and has no distinct diurnal cycle, whereas at Yala the wind speed exhibit a strong diurnal cycle with wind speeds ≥ 5 m s^{-1} occurring in the afternoon during the entire snow season. Dadic et al., (2013) found values around 3 – 5 m s^{-1} for a glaciered catchment in Switzerland. However, typical average values may not represent the actual wind conditions and thus DDF_H on a certain day. While for example the geometric mean of observed daily wind speed at the Brunnenkopfhütte station is about 0.8 m s^{-1} resulting in a DDF_H of approx. 0.7 mm °C^{-1} d^{-1}, the maximum daily average wind speed is about 4.5 m s^{-1} which increases DDF_H to approx. 3.9 mm °C^{-1} d^{-1}.

Table 3 Sensible heat component (DDF_H) [mm °C^{-1} d^{-1}] for selected wind speed (u) [m s^{-1}]

Wind Speed (u)	0.1	0.5	1.0	2.0	3.0	4.0	5.0	10.0
DDF_H	0.09	0.43	0.86	1.73	2.59	3.46	4.32	8.64

4.4 Latent heat component - DDF_E

The latent heat flux Q_E approximated by an aerodynamic model as in eq. (28) shows, that the latent heat component DDF_E is dependent on the humidity gradient near the snow surface and proportional to the wind speed. Table 4 and Figure 6 give the resulting DDF_E as a function of degree-days for different values of relative humidity and an average daily wind speed of $u = 1.0$ m s^{-1}. As with the sensible heat component DDF_H, DDF_E for any other wind speed can be obtained by multiplication with the actual value. For relative humidity < 30% the DDF_E is negative over the whole range of degree-days, hence the latent heat component will reduce the total DDF under these conditions. Even if the air is humid and warm, contribution of latent heat is moderate, e.g. DDF_E =1.05 mm °C^{-1} d^{-1} at a relative humidity of 100% and $T_{DD} = 20$ °C d.

In general, humid air will promote condensation at a cooler snow surface, which releases latent energy and contributes to a positive DDF, while dry air will promote evaporation and sublimation from the snow surface, which abstracts energy from the snowpack. Especially in spring, when relative humidity

is comparatively low in middle and northern latitudes, large parts of the incoming solar radiation can be consumed by evaporation from the snow surface reducing significantly the energy available for melt

530   and thus reducing the corresponding *DDFs* (Lang and Braun, 1990; Zhang et al., 2006).

Table 4 Latent heat component (DDF$_E$) [mm °C^{-1} d^{-1}] for selected relative humidity [%]

| | DDF$_E$ | | | | | | | | |
| | Relative Humidity | | | | | | | | |
T_{DD} [°C d]	10%	20%	30%	40%	50%	60%	70%	80%	90%	100%
1	-7.28	-6.40	-5.53	-4.66	-3.78	-2.91	-2.04	-1.16	-0.29	0.58
2	-3.61	-3.14	-2.67	-2.21	-1.74	-1.27	-0.80	-0.33	0.13	0.60
3	-2.38	-2.05	-1.72	-1.38	-1.05	-0.72	-0.38	-0.05	0.29	0.62
4	-1.77	-1.50	-1.23	-0.97	-0.70	-0.43	-0.16	0.10	0.37	0.64
5	-1.40	-1.17	-0.94	-0.71	-0.49	-0.26	-0.03	0.20	0.43	0.66
6	-1.15	-0.95	-0.75	-0.54	-0.34	-0.14	0.07	0.27	0.47	0.68
7	-0.98	-0.79	-0.61	-0.42	-0.23	-0.05	0.14	0.33	0.51	0.70
8	-0.84	-0.67	-0.50	-0.32	-0.15	0.03	0.20	0.37	0.55	0.72
9	-0.74	-0.58	-0.41	-0.25	-0.08	0.08	0.25	0.41	0.58	0.74
10	-0.66	-0.50	-0.34	-0.18	-0.02	0.13	0.29	0.45	0.61	0.77
15	-0.40	-0.26	-0.11	0.03	0.18	0.32	0.47	0.61	0.75	0.90
20	-0.26	-0.12	0.03	0.18	0.32	0.47	0.61	0.76	0.90	1.05

Note: These values are for u=1 m s^{-1}, for a different wind speed these values can be multiplied for desired wind speed.
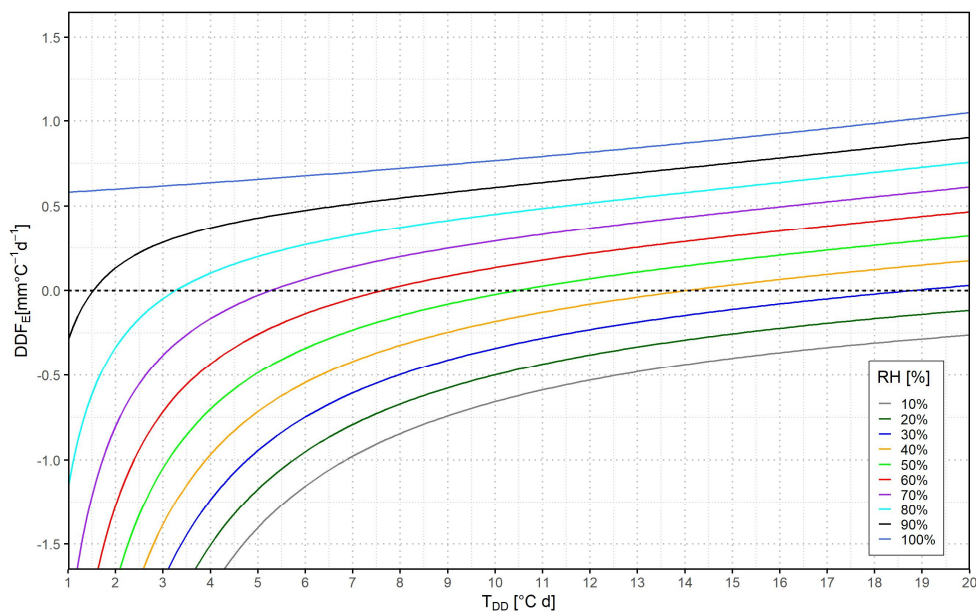
Figure 6 Latent Heat component (DDF$_E$) for selected relative humidity [%] and wind speed u = 1 m s^{-1}

535   *Note: These values are for u=1 m s^{-1}, for a different wind speed these values can be multiplied for desired wind speed.*

4.5 Precipitation heat component – DDF$_P$

Rainfall can affect the snowpack energy budget by adding sensible heat due to warm rain and by release of latent heat if the rain is frozen in the snowpack (DeWalle and Rango, 2008). The latter effect is not

540   considered in this study, as the snowpack is assumed at 0 °C melting condition. Because according to eq. (31) the precipitation heat Q_P is linearly dependent on air temperature, division by respective degree-days makes DDF$_P$ independent of temperature and proportional to rainfall, resulting in a DDF$_P$ = 0.0125 mm °C^{-1} d^{-1} for a precipitation depth of 1 mm per day. DDF$_P$ for any other precipitation can be obtained by respective multiplication. The exemplary values in Table 5 show however, that the contribution of

545   precipitation heat component DDF$_P$ is modest compared to other DDF components. Even high rainfall of 50 mm in a day would release only a small amount of sensible heat, resulting in a DDF$_P$ of 0.6 mm °C^{-1} d^{-1}.

Table 5 Precipitation heat component (DDF$_P$) [mm °C^{-1} day^{-1}] for selected precipitation [mm d^{-1}]

Precipitation (P)	1	2	5	10	25	50
DDF$_P$	0.0125	0.025	0.0625	0.125	0.313	0.625

4.6 DDF estimates comparison

550   In addition to the discussion on individual DDF components in previous sections, resulting total *DDFs* estimated from energy flux approaches are compared with observed *DDFs* at the Brunnenkopfhütte snow station. For this purpose, observed melt was estimated from the daily difference of observed snow water equivalent during melt periods (see Figure 7). Energy flux based melt was calculated by the formulas given in Sec. 3 using observed daily data from the Brunnenkopfhütte snow station (e.g. air

555   temperature, wind speed, etc.) where applicable. Monthly averages of observed data (November 2016 – May 2021) can be found inTable 1.

As in operational degree-day models typically at least 10-daily constant degree-day factors are used, both, energy flux based and observed daily melt values were accumulated on 10-daily basis and divided by the degree-days of the respective period. This averaging procedure also smooths daily noise in the

560   observed data, in particular inaccuracies in the determination of observed daily melt and unrealistic *DDF* values because of daily temperature averages just above 0 °C.

The comparison between observed and simulated (energy flux based) *DDFs* (see Figure 8) yields a fair agreement with BIAS = 0.2 mm °C^{-1} d^{-1} and RMSE = 1.1 mm °C^{-1} d^{-1}. Snowmelt periods in which a new snow event occurred (marked by hollow circles in Figure 8) were excluded from the calculation of

565   the error metrics, since new snow events contradict the condition that the snowpack is ripe and isothermal at 0 °C. Fresh snow increases the cold content of the snowpack and a certain amount of the incoming energy is needed to bring it back to 'ripe' conditions, thus is not available for melt. This effect can be clearly seen in Figure 8, since all simulated *DDFs* belonging to periods with new snow events considerably overestimate the observed *DDFs*. Taking into account such changes in the internal energy

570 of the snowpack under limited data availability would require a suitable parametrisation as discussed in Sec. 3.2.7, which is beyond the scope of the present study but may be subject to further research.
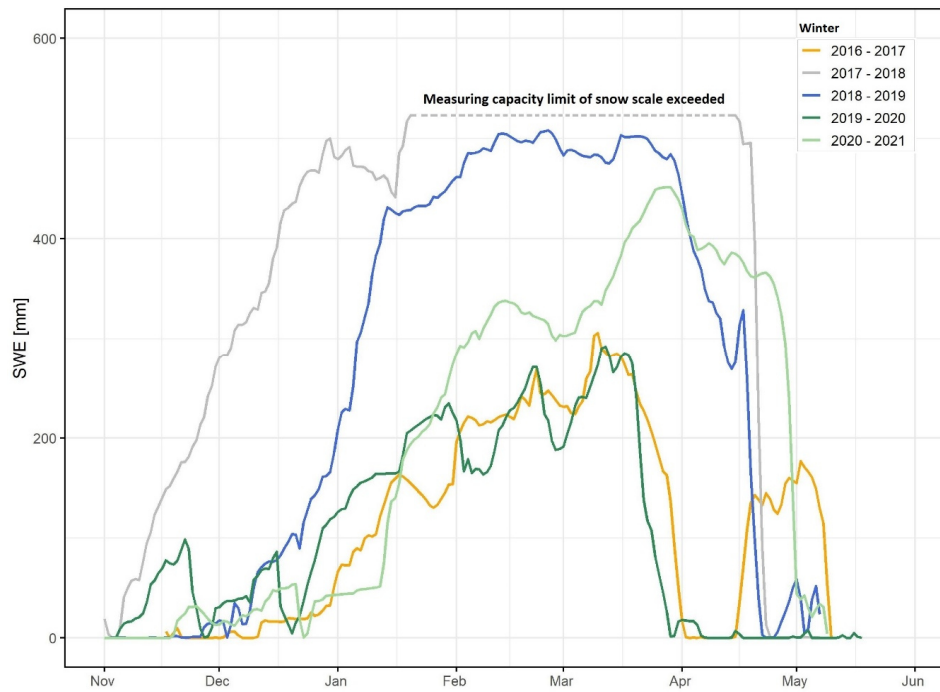
Figure 7 Observed snow water equivalent (SWE) at the Brunnenkopfhütte snow station (period: Winter 2016/2017 – 2020/2021)
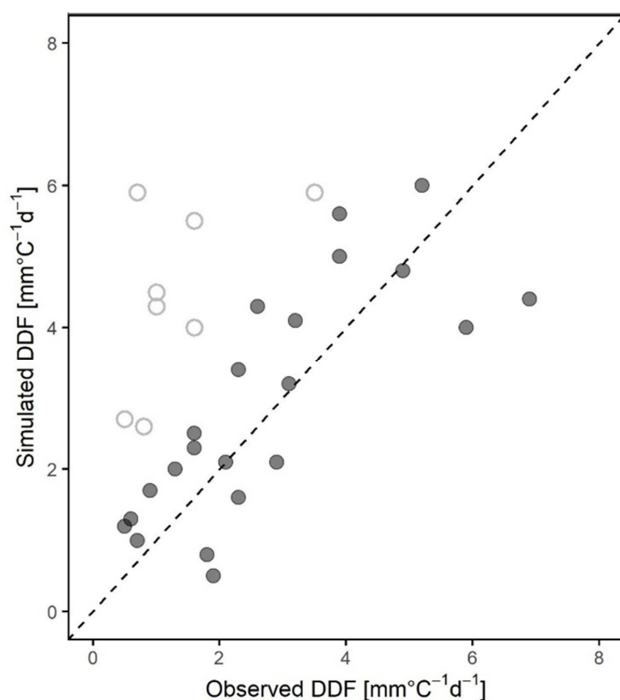
Figure 8 Comparison of observed vs simulated (energy flux based) 10-daily *DDF* for the Brunnenkopfhütte snow station (period: November 2016 – May 2021) – Hollow points represent *DDFs* during periods with new snow events

5. Discussion

While in the previous section the characteristic of each energy flux based DDF component is presented individually, in this section the influence of spatial, seasonal or meteorological conditions on the overall *DDF* is discussed. As before, all conclusions are under the assumption that the snowpack to isothermal at $T_s = 0$ °C and in ripe condition, hence all net incoming energy is available for melt and contributes to the total *DDF*. Other than the discussed variables are assumed constant with standard values $u = 1$ m s^{-1}, $RH = 70\%$, $A = 0.5$, $P = 0$ mm, latitude = 48° North (Brunnenkopfhütte snow station), and typical melt conditions of $T_{DD} = 5$ °C d if not stated otherwise.

5.1 Influence of latitude

Whereas local spatial variability in mountainous regions heavily affects melt by topographic effects, such as slope, aspect and shading, regional patterns of *DDFs* could not be detected in the data review by Hock, (2003). This observation is supported by a brief analysis of the effect of latitude where the *DDF* is compared not on the same date but at comparable melt conditions. The example compares typical melt conditions of $T_{DD} = 5$ °C d at latitude 35° North (Naran station, Upper Jhelum catchment) (Bogacki and Ismail, 2016), which usually occur around mid-February, with similar conditions at a higher latitude of 48° (Brunnenkopfhütte) that arrive about one month later in mid-March. Figure 9 (a)

595   shows that the decisive solar radiation component is very similar in both situations, thus the total *DDF* is virtually identical at both locations. Therefore, at least in moderate latitudes, there is no significant effect of latitude on *DDF* when compared under similar melt conditions.

5.2 Influence of altitude

Contrary to the compensating effect in the case of latitude, the delayed onset of snowmelt due to altitude
600   influences the *DDF* noticeably, which becomes important in temperature-index models where calculation is usually based on elevation bands. In order to demonstrate the influence of altitude on the *DDF*, two elevation zones with an altitude of 2000 and 4000 m a.s.l. respectively are compared near Naran station in the Upper Jhelum catchment. As already mentioned, typical melt conditions of $T_{DD} = 5$ °C d occur at Naran usually around mid-February, while at 4000 m a.s.l. similar degree-days arrive
605   about mid-May. The resulting *DDFs* (Figure 9 (b)) show a significant difference, both under clear sky as under overcast conditions, because of the different input in solar radiation caused by the alteration in solar angle.

Figure 9 (b) shows an additional term DDF_A on top of the solar radiation component that represents the increase in incoming solar radiation due to the clearness altitude factor, which takes into account the
610   increase of the clearness index with altitude. Averaging the factors proposed by different solar radiation models (see Figure 4) results in an additional component DDF_A of 0.4 and 1.4 mm °C^{-1} d^{-1} under clear sky and of 0.5 and 1.6 mm °C^{-1} d^{-1} und overcast conditions at 2000 and 4000 m a.s.l. respectively.

While for exemplification, snow albedo is assumed constant at 0.5 in Figure 9 (b), taking into consideration the decrease of albedo as the snow ages e.g. $A = 0.74$ in February and $A = 0.42$ in May
615   results in a more pronounced difference with altitude, i.e. a total *DDF* of 0.3 compared to 10.5 mm °C^{-1} d^{-1} under clear sky and of 2.7 versus 7.3 mm °C^{-1} d^{-1} under overcast conditions for the two altitudes respectively.

5.3 Influence of albedo

As already discussed in the sections before, snow albedo is a critical parameter for the *DDF* since
620   according eq. (5) albedo directly controls the net solar radiation flux into the snowpack. While albedo of fresh snow is well above 0.9 hence reflecting most of the incoming shortwave radiation, it drops rapidly when larger grains form due to snow metamorphism. Figure 9 (c) demonstrates the effect of aging snow after a new snow event, when a simple exponential decay model as given in eq. (19) is used and typical melting conditions $T_{DD} = 5$ °C d are assumed. Since directly after a new snow event (Day =
625   0) the fresh snow albedo is high ($A = 0.95$), the overall *DDF* is generally small. Under clear sky conditions, in case longwave radiation cooling is larger than net shortwave radiation flux, even a negative *DDF* value, i.e. no melt, may occur. If there is no new snow event in-between, albedo will decrease following the exponential decay model to 0.52 after 10 days resulting in a *DDF* of 5.8 mm °C^{-1} d^{-1} under clear sky and 4.4 mm °C^{-1} d^{-1} under overcast conditions. As described qualitatively in the

630   literature e.g. (Hock, 2003), under all sky conditions the *DDF* is continuously increasing with decreasing albedo, with the increase however being more pronounced under clear sky than under overcast conditions.

5.4 Influence of season

Since the solar angle is rising from its minimum at winter solstice in December to its maximum on 21th

635   June, the solar radiation component DDF$_S$ is increasing during the snowmelt season and thus the *DDF* is expected to increase respectively. Figure 9 (d) shows the influence of season on the *DDF* at Brunnenkopfhütte snow station during the melt period, assuming average degree-days of 1, 4, and 7 °C d in March, April, and May respectively (seeTable 1). Under clear sky conditions, as expected total *DDF* increases from a negative value of -3.6 mm °C^{-1} d^{-1} in March to 6.6 mm °C^{-1} d^{-1} in May. Under

640   overcast conditions however, the *DDF* is virtually stable ranging from 4.4 to 4.5 mm °C^{-1} d^{-1} in the same period.

An evaluation of the individual DDF components shows, that under clear sky conditions the high impact of solar radiation in combination with low degree-days at the onset of the snowmelt season is counterweighted by a strong negative longwave radiation component that decreases as the season

645   progresses. Under overcast conditions, DDF$_L$ is neutral or slightly positive while the DDF$_S$ component decreases because degree-days are rising faster than solar radiation input, which implies that sky conditions are more decisive for an estimate of the *DDF* than the date.

The effect of cloud cover is further amplified by the decrease in albedo while the melt season progresses, which becomes more significant under clear sky conditions. In the present example, that uses the average

650   monthly albedo as specified inTable 1, only 30% of incoming solar radiation is contributing to melt in March, while it is about 60% in May, enhancing the marked increase of *DDF* under clear sky conditions.

5.5 Rain on snow events

In general, precipitation heat component alone has only a minor effect on the *DDF*. However, in conjunction with certain weather conditions like braking in of warm and moist air, rain over snow events

655   may lead to sudden melt and severe flooding. In a well-documented event in the Alps in October 2011 (Rössler et al., 2014) intensive rainfall (on average 100 mm d^{-1}) was accompanied by an increase in temperature by 9 °C, which shifted the 0 °C line from 1500 to 3200 m a.s.l. during one day. Similar conditions occurred e.g. end-December 2021 in Switzerland, when after the establishment of a solid snow cover, an Atlantic cyclone caused a sudden temperature rise up to 19 °C, wind gusts of 35 – 40 m

660   s^{-1} and locally more than 70 mm precipitation (MeteoSchweiz, 2022), which e.g. at Adelboden (1325 m a.s.l.) caused the complete melt of an approx. 40 cm snow cover.

Figure 9 (e) shows the different DDF components resulting from a hypothetical rain over snow event assuming an air temperature of 15 °C, a precipitation of 70 mm d^{-1}, an average daily wind speed of 10 m s^{-1}, a relative humidity of 100%, and overcast conditions. Although the amount of precipitation is

665 substantial and rain's temperature is comparatively high, the contribution of DDF_P is still modest. However, air temperature, relative humidity, and in particular wind speed associated with such events increase the sensible and latent heat components significantly. Thus, the resulting overall *DDF* is much higher than under usual melt conditions, which may lead to a considerable melt that adds to the runoff already caused by the heavy rain.

(a)

670

(b)

(c)
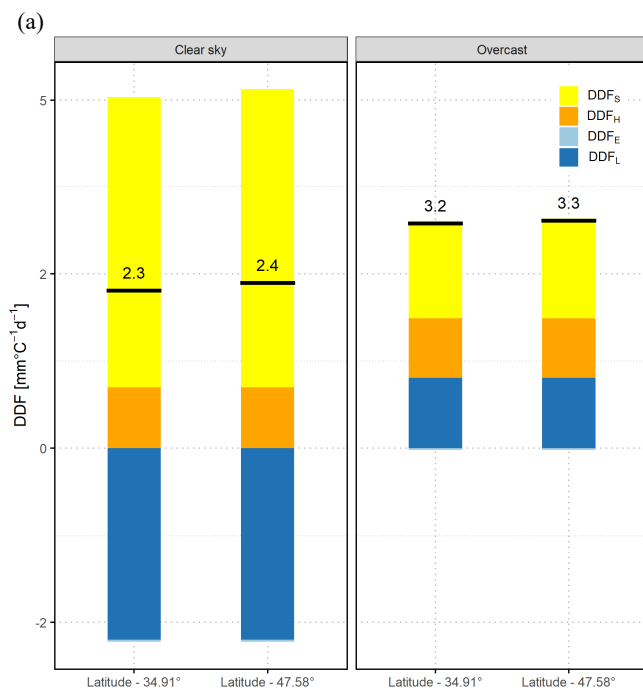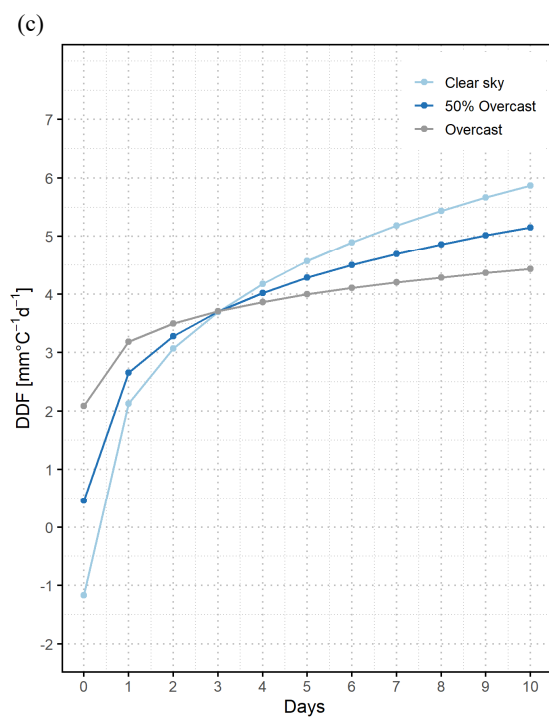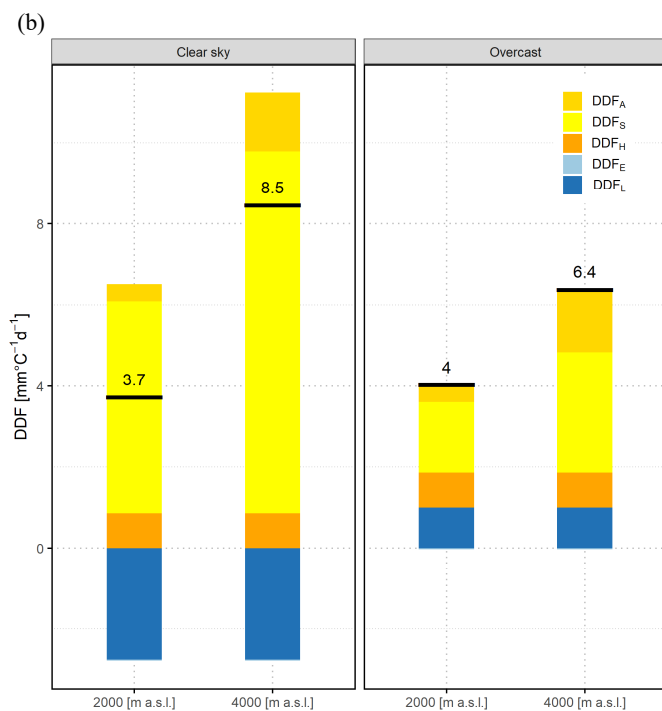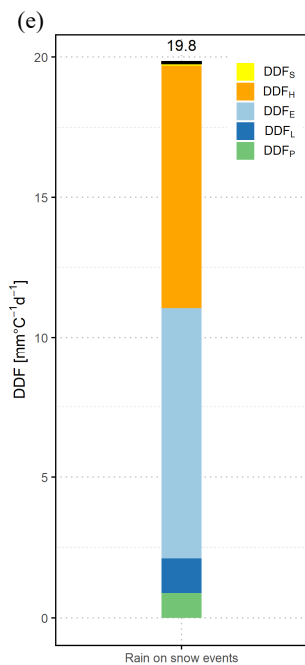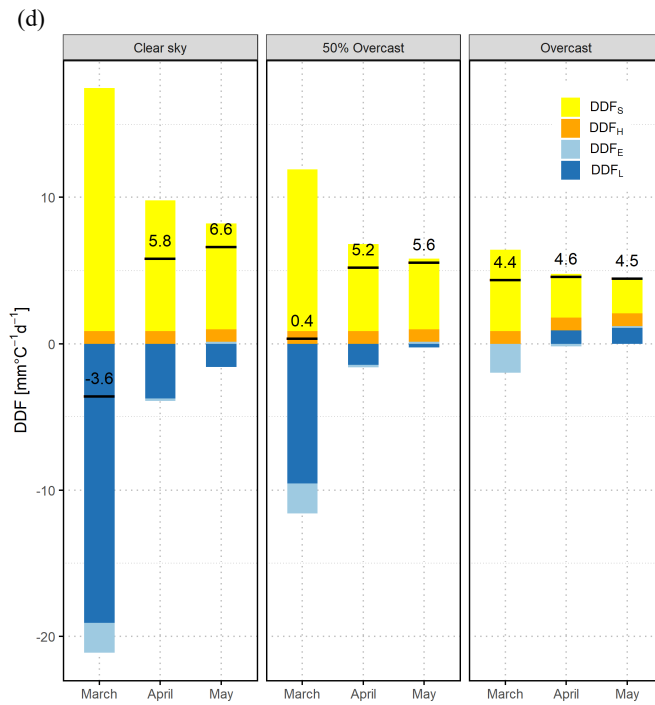
675   Figure 9 Influence of (a) latitude (b) altitude (c) albedo (d) season (e) rain on snow events – on the *DDF*

5.6 DDF estimation for temperature-index modelling

Snowmelt runoff models using the temperature-index approach have proven useful tools for simulation and forecasting in large snow or glacier dominated catchments, in particular in remote mountainous regions where data is usually scarce. A good estimate of the degree-day factor as the decisive model parameter is important either to stay in a realistic range when calibrating this parameter or in case of forecasting when estimating its changes while the season progresses. In order to demonstrate the alteration of *DDFs* over time and altitude, energy flux based *DDFs* are estimated using 10-daily average temperature (i.e. period 2000 – 2015) for the key elevation zones in the Upper Jhelum catchment (Bogacki and Ismail, 2016). Because of the lack of other than temperature and precipitation data, prevailing conditions during the melt season are crudely approximated by the standard conditions used in this section, assuming persistent clear sky conditions and albedo declining according eq. (19) after last fresh snow just before the beginning of the melting period.

Figure 10 (a) shows the development of *DDFs* in the elevation zones over time. As expected, melt starts earlier in lower elevation zones and successively progresses to higher altitudes. Interestingly, the *DDF* in the first 10-daily period of melting in each elevation zone increases with altitude. Obviously this is a combined effect of higher solar radiation input and decreasing albedo while the season progresses and the circumstance that the onset of melt in higher elevation zones starts at a lower degree-day threshold than in lower zones. In contrast to Figure 9 (d), the *DDF* decreases continuously in all elevation zones in the subsequent melting periods since air temperature and thus degree-days rise faster than melt increases.

5.7 Influence of climate change

Climate change will ultimately influence snowmelt patterns depending on the projected changes in temperature and precipitation. In recent studies, usually model parameters including *DDFs* are considered as constant when assessing the climate change impact on future water availability from snow and glacier fed catchments (Lutz et al., 2016; Hasson et al., 2019; Ismail et al., 2020). However, due to the physical processes on which they depend these parameters are subject to climate change. In this section, an attempt is made to estimate the influence of climate change on the *DDFs* in different elevation zones. For this analysis, projected temperature changes for the period 2071 – 2100 that according to data for the Upper Indus Basin (Ismail et al., 2020) amount to $\Delta T = 2.3$ °C under RCP2.6 and to $\Delta T = 6.5$ °C under RCP8.5 are added to the temperatures in present climate for each elevation zone.

The first effect to be observed in Figure 10 (b) and (c) is the common finding that snowmelt will start earlier under climate change as temperatures rise earlier above freezing. In addition, since being earlier in the year, the *DDFs* in corresponding elevation zones are generally smaller compared to the current climate, though there are some outliers at the start of melting, due to division by low degree-day values. In case of the pessimistic scenario RCP8.5 (Figure 10 (c)), a seasonal snow cover will not establish any

more in the lowest elevation zone (i.e. 2500 – 3000 m a.s.l.) as air temperature at this altitude is projected to stay well above freezing throughout the winter. In general, the results of this brief analysis indicate, that the *DDFs* are expected to decrease under the influence of climate change, as melt will occur earlier

715   in the year when solar radiation is smaller.
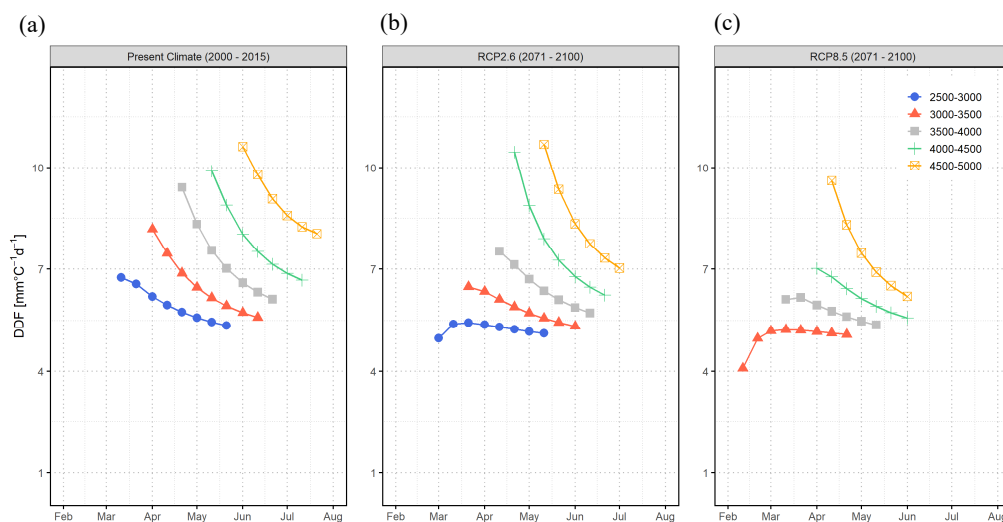
Figure 10(a) DDF estimation for a temperature-index modelling (b) Influence of climate change – 2071 – 2100 under RCP2.6 (c) Influence of climate change – 2071 – 2100 under RCP8.5

720   **6. Conclusions**

Degree-day models are common and valuable tools for assessing present and future water availability in large snow or glacier melt dominated basis, in particular when data is scarce like e.g. in the Hindukush-Karakoram-Himalayas mountain ranges. The present study attempts to quantify the effects of spatial, temporal, and climatic conditions on the degree-day factor (*DDF*), in order to gain a better

725   understanding which influencing factors are decisive under which conditions. While this analysis is physically based on the energy balance, approximate formulas for estimating the *DDFs* are used to account for situations where observed data is limited. In addition, resulting tables and graphs for typical melt conditions are provided for a quick assessment.

A comparison between observed and estimated *DDFs* at the Brunnenkopfhütte snow station shows a

730   fair agreement with BIAS = 0.2 mm °C^{-1} d^{-1} and RMSE = 1.1 mm °C^{-1} d^{-1} that however only takes into account periods without new snow events, since fresh snow increases the cold content of the snowpack and contradicts the condition of the snowpack being ripe and isothermal at 0 °C. If, under the constraint of limited data availability, also changes in the cold content of the snowpack shall be considered, further research is needed on an approach that sufficiently parameterizes the diurnal dynamic of vertical

735   temperature distribution in the snowpack.

Furthermore, it is neither intended to use these *DDF* estimates directly as a model parameter nor to incorporate an energy balance based *DDF* approach into a degree-day model. One important aspect of temperature-index models is, that the *DDF* is a lumped parameter, which is usually subject to calibration and accounts for uncertainties in different variables and parameters, e.g. temperature estimates, runoff

740   coefficients, etc. Thus, the *DDF* estimated by the energy balance approach are rather aimed to validate the results of parameter calibration or to indicate necessary adjustments due to climate change.

The analysis of the energy balance processes controlling snowmelt indicates that cloud cover is the most decisive factor for the dynamics of the *DDF*. Under overcast conditions, the contribution of shortwave radiation is comparatively low whereas the other components are in general small. Therefore, total *DDF*

745   is moderate and variations due to other factors are usually limited, apart from exceptional rainstorm events, for which however energy balance models are the more suitable approach.

Under clear sky conditions on the other hand, shortwave radiation is the most prominent component contributing to melt. The increase of solar angle while the melt season progresses in combination with declining albedo and a decreasing cooling effect by the longwave radiation component along with

750   increasing air temperature leads to a pronounced temporal dynamic in the *DDF*. Whereas incoming solar radiation and net longwave radiation can be determined fairly accurate under clear sky conditions, albedo becomes the crucial parameter for estimating the *DDF*, especially when new snow events occur during the melt period.

Clear sky conditions promote the effect of increasing *DDF* with altitude if similar melting conditions

755   are compared, since melting temperatures arrive later in the season at higher altitudes. The opposite effect can be observed with regard to climate change. It is well known and because of higher temperature evident, that at a certain altitude climate change will shift the snowmelt season earlier in the year. Consequently, when comparing periods of similar degree-days, as results from this study indicate the *DDFs* are expected to decrease, since solar radiation is lower and albedo is likely to be higher.

760   Therefore, and as pointed out by many researchers, the *DDF* cannot be considered a constant model parameter. Rather, its spatial and temporal variability must be taken into account especially when using temperature-index models for forecasting present or predicting future water availability.

Author contributions

765 **MFI:** Conceptualization, Methodology, Software, Formal analysis, Investigation, Data curation, Writing – original draft, editing, Visualization. **WB:** Conceptualization, Methodology, Software, Formal analysis, Investigation, Data curation, Writing – reviewing & editing. **MD:** Supervision, review & editing. **MS:** Data curation, review & editing, **LK:** Supervision, Data curation.

Competing Interest

770 The contact author has declared that neither they nor their co-authors have any competing interests.

Acknowledgements

We thank Koblenz University of Applied Sciences that we could use the data of the snow station for this study.

7. References

Ahmad, M. J. and Tiwari, G. N.: Solar radiation models-A review, Int. J. Energy Res., 35, 271–290, https://doi.org/10.1002/er.1690, 2011.

Allen, R. G., Pereira, L. S., Raes, D., and Smith, M.: Crop evapotranspiration —guidelines for computing crop water requirements, FAO, 56, 1998.

Ambach, W.: Characteristics of the Heat Balance of the Greenland Ice sheet for Modelling, J. Glaciol., 31, 3–12, https://doi.org/10.3189/S0022143000004925, 1985.

Anderson, E. A.: National Weather Service river forecast system: snow accumulation and ablation model, https://repository.library.noaa.gov/view/noaa/13507, 1973.

Anderson, E. A.: Snow Accumulation and Ablation Model - SNOW-17, NOAA's National Weather Service, Office of Hydrologic Development, Silver Spring, 2006.

Annandale, J., Jovanovic, N., Benadé, N., and Allen, R.: Software for missing data error analysis of Penman-Monteith reference evapotranspiration, Irrigation Science, 21, 57–67, https://doi.org/10.1007/s002710100047, 2002.

Arendt, A. A. and Sharp, M. J.: Energy balance measurements on a Canadian high Arctic glacier and their implications for mass balance modelling, IAHS-AISH publication, 165–172, 1999.

Asaoka, Y. and Kominami, Y.: Incorporation of satellite-derived snow-cover area in spatial snowmelt modeling for a large area: determination of a gridded degree-day factor, Ann. Glaciol., 54, 205–213, https://doi.org/10.3189/2013AoG62A218, 2013.

Badescu, V. and Paulescu, M.: Statistical properties of the sunshine number illustrated with measurements from Timisoara (Romania), Atmospheric Research, 101, 194–204, https://doi.org/10.1016/j.atmosres.2011.02.009, 2011.

Bagchi, A. K.: Areal value of degree-day factor / Valeur spatiale du facteur degré-jour, Hydrological Sciences Journal, 28, 499–511, https://doi.org/10.1080/02626668309491991, 1983.

Bergström, S.: Development and application conceptual runoff model for scandinavian catchments, SMHI, Research Department, Hydrology, 162, 1976.

Bogacki, W. and Ismail, M. F.: Seasonal forecast of Kharif flows from Upper Jhelum catchment, Proc. IAHS, 374, 137–142, https://doi.org/10.5194/piahs-374-137-2016, 2016.

Bormann, K. J., Evans, J. P., and McCabe, M. F.: Constraining snowmelt in a temperature-index model using simulated snow densities, Journal of Hydrology, 517, 652–667, https://doi.org/10.1016/j.jhydrol.2014.05.073, 2014.

Braithwaite, R. J.: Positive degree-day factors for ablation on the Greenland ice sheet studied by energy-balance modelling, J. Glaciol., 41, 153–160, https://doi.org/10.3189/S0022143000017846, 1995.

Braithwaite, R. J.: Temperature and precipitation climate at the equilibrium-line altitude of glaciers expressed by the degree-day factor for melting snow, J. Glaciol., 54, 437–444, https://doi.org/10.3189/002214308785836968, 2008.

Braithwaite, R. J., Konzelmann, T., Marty, C., and Olesen, O. B.: Reconnaissance Study of glacier energy balance in North Greenland, 1993–94, J. Glaciol., 44, 239–247, https://doi.org/10.3189/S0022143000002586, 1998.

Braun, L. N.: Simulation of snowmelt-runoff in lowland and lower alpine regions of Switzerland, Ph.D. Thesis, ETH Zurich, https://doi.org/10.3929/ETHZ-A-000334295, 1984.

Braun, Ludwig., Grabs, W., and Rana, B.: Application of a Conceptual Precipitation Runoff Model in the Langtang Kfaola Basin, Nepal Himalaya, Snow and Glacier Hydrology, 1993.

Bristow, K. L. and Campbell, G. S.: On the relationship between incoming solar radiation and daily maximum and minimum temperature, Agricultural and Forest Meteorology, 31, 159–166, https://doi.org/10.1016/0168-1923(84)90017-0, 1984.

Brutsaert, W.: On a derivable formula for long-wave radiation from clear skies, Water Resour. Res., 11, 742–744, https://doi.org/10.1029/WR011i005p00742, 1975.

Brutsaert, W.: Evaporation into the Atmosphere, Springer Netherlands, Dordrecht, https://doi.org/10.1007/978-94-017-1497-6, 1982.

Campbell, G. S. and Norman, J. M.: Introduction to environmental biophysics, 2nd ed., Springer, New York, 286 pp., 1998.

Dadic, R., Mott, R., Lehning, M., Carenzo, M., Anderson, B., and Mackintosh, A.: Sensitivity of turbulent fluxes to wind speed over snow surfaces in different climatic settings, Advances in Water Resources, 55, 178–189, https://doi.org/10.1016/j.advwatres.2012.06.010, 2013.

DeWalle, D. R. and Rango, A.: Principles of Snow Hydrology, Cambridge University Press, Cambridge, https://doi.org/10.1017/CBO9780511535673, 2008.

Doorenbos, J. and Pruitt, W. O.: Guidelines for predicting crop water requirements, Rev., Food and Agriculture Organization of the United Nations, Rome, 144 pp., 1977.

Ekici, C.: Total Global Solar Radiation Estimation Models and Applications: A review, IJITIS, 2, 212-228 Pages, https://doi.org/10.15157/IJITIS.2019.2.2.212-228, 2019.

Evrendilek, F. and Ertekin, C.: Assessing solar radiation models using multiple variables over Turkey, Clim Dyn, 31, 131–149, https://doi.org/10.1007/s00382-007-0338-6, 2008.

Gafurov, A.: Water balance modeling using remote sensing information: focus on Central Asia, Ph.D. Thesis, Inst. f. Wasserbau, Stuttgart, 116 pp., 2010.

Hargreaves, G. H. and Samani, Z. A.: Estimating Potential Evapotranspiration, J. Irrig. and Drain. Div., 108, 225–230, https://doi.org/10.1061/JRCEA4.0001390, 1982.

Harpold, A. A. and Brooks, P. D.: Humidity determines snowpack ablation under a warming climate, Proc Natl Acad Sci USA, 115, 1215–1220, https://doi.org/10.1073/pnas.1716789115, 2018.

Hasson, S. ul, Saeed, F., Böhner, J., and Schleussner, C.-F.: Water availability in Pakistan from Hindukush–Karakoram–Himalayan watersheds at 1.5 °C and 2 °C Paris Agreement targets, Advances in Water Resources, 131, 103365, https://doi.org/10.1016/j.advwatres.2019.06.010, 2019.

He, Z. H., Parajka, J., Tian, F. Q., and Blöschl, G.: Estimating degree-day factors from MODIS for snowmelt runoff modeling, Hydrol. Earth Syst. Sci., 18, 4773–4789, https://doi.org/10.5194/hess-18-4773-2014, 2014.

Hinzman, L. D. and Kane, D. L.: Snow hydrology of a headwater Arctic basin: 2. Conceptual analysis and computer modeling, Water Resour. Res., 27, 1111–1121, https://doi.org/10.1029/91WR00261, 1991.

Hock, R.: A distributed temperature-index ice- and snowmelt model including potential direct solar radiation, J. Glaciol., 45, 101–111, https://doi.org/10.3189/S0022143000003087, 1999.

Hock, R.: Temperature index melt modelling in mountain areas, Journal of Hydrology, 282, 104–115, https://doi.org/10.1016/S0022-1694(03)00257-9, 2003.

Hock, R.: Glacier melt: a review of processes and their modelling, Progress in Physical Geography: Earth and Environment, 29, 362–391, https://doi.org/10.1191/0309133305pp453ra, 2005.

Hock, R. and Noetzli, C.: Areal melt and discharge modelling of Storglaciären, Sweden, Ann. Glaciol., 24, 211–216, https://doi.org/10.3189/S0260305500012192, 1997.

Immerzeel, W. W., Droogers, P., de Jong, S. M., and Bierkens, M. F. P.: Large-scale monitoring of snow cover and runoff simulation in Himalayan river basins using remote sensing, Remote Sensing of Environment, 113, 40–49, https://doi.org/10.1016/j.rse.2008.08.010, 2009.

Ismail, M. F. and Bogacki, W.: Scenario approach for the seasonal forecast of Kharif flows from the Upper Indus Basin, Hydrol. Earth Syst. Sci., 22, 1391–1409, https://doi.org/10.5194/hess-22-1391-2018, 2018.

Ismail, M. F., Bogacki, W., and Muhammad, N.: Degree-day factor models for forecasting the snowmelt runoff for Naran watershed, SI, 27, 1951–1960, 2015.

Ismail, M. F., Naz, B. S., Wortmann, M., Disse, M., Bowling, L. C., and Bogacki, W.: Comparison of two model calibration approaches and their influence on future projections under climate change in the Upper Indus Basin, Climatic Change, 163, 1227–1246, https://doi.org/10.1007/s10584-020-02902-3, 2020.

Jansson, P., Hock, R., and Schneider, T.: The concept of glacier storage: a review, Journal of Hydrology, 282, 116–129, https://doi.org/10.1016/S0022-1694(03)00258-0, 2003.

Jennings, K. S., Kittel, T. G. F., and Molotch, N. P.: Observations and simulations of the seasonal evolution of snowpack cold content and its relation to snowmelt and the snowpack energy budget, The Cryosphere, 12, 1595–1614, https://doi.org/10.5194/tc-12-1595-2018, 2018.

Jin, Z., Yezheng, W., and Gang, Y.: General formula for estimation of monthly average daily global solar radiation in China, Energy Conversion and Management, 46, 257–268, https://doi.org/10.1016/j.enconman.2004.02.020, 2005.

Kane, D. L., Gieck, R. E., and Hinzman, L. D.: Snowmelt Modeling at Small Alaskan Arctic Watershed, Journal of Hydrologic Engineering, 2, 204–210, https://doi.org/10.1061/(ASCE)1084-0699(1997)2:4(204), 1997.

Kayastha, R. B., Yutaka, A., Masayoshi, N., Koji, F., Akiko, S., and Yoshihiro, M.: Positive degree-day factors for ice ablation on four glaciers in the Nepalese Himalayas and Qinghai-Tibetan Plateau, Bulletin of glaciological research, 7–14, 2003.

Klok, E. J., Jasper, K., Roelofsma, K. P., Gurtz, J., and Badoux, A.: Distributed hydrological modelling of a heavily glaciated Alpine river basin, Hydrological Sciences Journal, 46, 553–570, https://doi.org/10.1080/02626660109492850, 2001.

Kopp, G. and Lean, J. L.: A new, lower value of total solar irradiance: Evidence and climate significance: FRONTIER, Geophys. Res. Lett., 38, n/a-n/a, https://doi.org/10.1029/2010GL045777, 2011.

Kopp, M., Tuo, Y., and Disse, M.: Fully automated snow depth measurements from time-lapse images applying a convolutional neural network, Science of The Total Environment, 697, 134213, https://doi.org/10.1016/j.scitotenv.2019.134213, 2019.

Kustas, W. P., Rango, A., and Uijlenhoet, R.: A simple energy budget algorithm for the snowmelt runoff model, Water Resour. Res., 30, 1515–1527, https://doi.org/10.1029/94WR00152, 1994.

Lang, H.: Forecasting Meltwater Runoff from Snow-Covered Areas and from Glacier Basins, in: River Flow Modelling and Forecasting, vol. 3, edited by: Kraijenhoff, D. A. and Moll, J. R., Springer Netherlands, Dordrecht, 99–127, https://doi.org/10.1007/978-94-009-4536-4_5, 1986.

Lang, H. and Braun, L.: On the information content of air temperature in the context of snow melt estimation, IAHS, 190, 347–354, 1990.

Lawrence, M. G.: The Relationship between Relative Humidity and the Dewpoint Temperature in Moist Air: A Simple Conversion and Applications, Bull. Amer. Meteor. Soc., 86, 225–234, https://doi.org/10.1175/BAMS-86-2-225, 2005.

Lehning, M., Bartelt, P., Brown, B., and Fierz, C.: A physical SNOWPACK model for the Swiss avalanche warning, Cold Regions Science and Technology, 35, 169–184, https://doi.org/10.1016/S0165-232X(02)00072-1, 2002.

Liu, Y., Tan, Q., and Pan, T.: Determining the Parameters of the Ångström-Prescott Model for Estimating Solar Radiation in Different Regions of China: Calibration and Modeling, Earth and Space Science, 6, 1976–1986, https://doi.org/10.1029/2019EA000635, 2019.

Luo, Y., Arnold, J., Liu, S., Wang, X., and Chen, X.: Inclusion of glacier processes for distributed hydrological modeling at basin scale with application to a watershed in Tianshan Mountains, northwest China, Journal of Hydrology, 477, 72–85, https://doi.org/10.1016/j.jhydrol.2012.11.005, 2013.

Lutz, A. F., Immerzeel, W. W., Kraaijenbrink, P. D. A., Shrestha, A. B., and Bierkens, M. F. P.: Climate Change Impacts on the Upper Indus Hydrology: Sources, Shifts and Extremes, PLoS ONE, 11, e0165630, https://doi.org/10.1371/journal.pone.0165630, 2016.

Marks, D., Dozier, J., and Davis, R. E.: Climate and energy exchange at the snow surface in the Alpine Region of the Sierra Nevada: 1. Meteorological measurements and monitoring, Water Resour. Res., 28, 3029–3042, https://doi.org/10.1029/92WR01482, 1992.

Marks, D., Domingo, J., Susong, D., Link, T., and Garen, D.: A spatially distributed energy balance snowmelt model for application in mountain basins, Hydrol. Process., 13, 1935–1959, https://doi.org/10.1002/(SICI)1099-1085(199909)13:12/13<1935::AID-HYP868>3.0.CO;2-C, 1999.

Marsh, C. B., Pomeroy, J. W., and Spiteri, R. J.: Implications of mountain shading on calculating energy for snowmelt using unstructured triangular meshes: Implication of Mountains shading for snowmelt, Hydrol. Process., 26, 1767–1778, https://doi.org/10.1002/hyp.9329, 2012.

Martinec, J.: The degree-day factor for snowmelt-runoff forecasting, 51, 468–477, 1960.

Martinec, J.: Snowmelt - runoff model for stream flow forecasts, 145–154, 1975.

Martinec, J., Rango, A., and Roberts, R.: Snowmelt Runoff Model (SRM) User's Manual, 180, 2008.

Masters, G. M.: Renewable and efficient electric power systems, John Wiley & Sons, Hoboken, NJ, 654 pp., 2004.

Matthews, T. and Hodgkins, R.: Interdecadal variability of degree-day factors on Vestari Hagafellsjökull (Langjökull, Iceland) and the importance of threshold air temperatures, J. Glaciol., 62, 310–322, https://doi.org/10.1017/jog.2016.21, 2016.

McGinn, R. A.: Degree-day snowmelt runoff experiments; Clear Lake Watershed, Riding Mountain National Park, Geographical Essays, 15, 16, 2012.

Meeus, J.: Astronomical algorithms, 1st English ed., Willmann-Bell, Richmond, Va, 429 pp., 1991.

MeteoSchweiz: MeteoSchweiz - Klimabulletin Dezember 2021, https://www.meteoschweiz.admin.ch/home/aktuell/news.subpage.html/de/data/news/2022/1/wetterrue ckblick-dezember-mit-viel-hochnebel.html, 2022.

Monteith, J. L. and Unsworth, M. H.: Principles of environmental physics: plants, animals, and the atmosphere, 4th ed., Elsevier/Academic Press, Amsterdam ; Boston, 401 pp., 2013.

Murray, F. W.: On the Computation of Saturation Vapor Pressure, J. Appl. Meteor., 6, 203–204, https://doi.org/10.1175/1520-0450(1967)006<0203:OTCOSV>2.0.CO;2, 1967.

Oke, T. R.: Boundary Layer Climates, 0 ed., Routledge, https://doi.org/10.4324/9780203407219, 1987.

Pelkowski, J.: A physical rationale for generalized Ångström–Prescott regression, Solar Energy, 83, 955–963, https://doi.org/10.1016/j.solener.2008.12.011, 2009.

Pellicciotti, F., Brock, B., Strasser, U., Burlando, P., Funk, M., and Corripio, J.: An enhanced temperature-index glacier melt model including the shortwave radiation balance: development and testing for Haut Glacier d'Arolla, Switzerland, J. Glaciol., 51, 573–587, https://doi.org/10.3189/172756505781829124, 2005.

Prasad, V. H. and Roy, P. S.: Estimation of Snowmelt Runoff in Beas Basin, India, Geocarto International, 20, 41–47, https://doi.org/10.1080/10106040508542344, 2005.

Quick, M. C. and Pipes, A.: U.B.C. Watershed model / Le modèle du bassin versant U.C.B, Hydrological Sciences Bulletin, 22, 153–161, https://doi.org/10.1080/02626667709491701, 1977.

Rango, A. and Martinec, J.: Application of a Snowmelt-Runoff Model Using Landsat Data, 10, 225–238, https://doi.org/10.2166/nh.1979.0006, 1979.

Rango, A. and Martinec, J.: Revisiting the degree-day method for snowmelt computations, J Am Water Resources Assoc, 31, 657–669, https://doi.org/10.1111/j.1752-1688.1995.tb03392.x, 1995.

Reda, I. and Andreas, A.: Solar position algorithm for solar radiation applications, Solar Energy, 76, 577–589, https://doi.org/10.1016/j.solener.2003.12.003, 2004.

Rensheng, C., Shihua, L., Ersi, K., Jianping, Y., and Xibin, J.: Estimating daily global radiation using two types of revised models in China, Energy Conversion and Management, 47, 865–878, https://doi.org/10.1016/j.enconman.2005.06.015, 2006.

Rössler, O., Froidevaux, P., Börst, U., Rickli, R., Martius, O., and Weingartner, R.: Retrospective analysis of a nonforecasted rain-on-snow flood in the Alps – a matter of model limitations or unpredictable nature?, Hydrol. Earth Syst. Sci., 18, 2265–2285, https://doi.org/10.5194/hess-18-2265-2014, 2014.

Schaefli, B. and Huss, M.: Integrating point glacier mass balance observations into hydrologic model identification, Hydrol. Earth Syst. Sci., 15, 1227–1241, https://doi.org/10.5194/hess-15-1227-2011, 2011.

Schmid, M.-O., Gubler, S., Fiddes, J., and Gruber, S.: Inferring snowpack ripening and melt-out from distributed measurements of near-surface ground temperatures, The Cryosphere, 6, 1127–1139, https://doi.org/10.5194/tc-6-1127-2012, 2012.

Schreider, S. Yu., Whetton, P. H., Jakeman, A. J., and Pittock, A. B.: Runoff modelling for snow-affected catchments in the Australian alpine region, eastern Victoria, Journal of Hydrology, 200, 1–23, https://doi.org/10.1016/S0022-1694(97)00006-1, 1997.

Shea, J. M., Dan Moore, R., and Stahl, K.: Derivation of melt factors from glacier mass-balance records in western Canada, J. Glaciol., 55, 123–130, https://doi.org/10.3189/002214309788608886, 2009.

Stigter, E. E., Steiner, J. F., Koch, I., Saloranta, T. M., Kirkham, J. D., and Immerzeel, W. W.: Energy and mass balance dynamics of the seasonal snowpack at two high-altitude sites in the Himalaya, Cold Regions Science and Technology, 183, 103233, https://doi.org/10.1016/j.coldregions.2021.103233, 2021.

Tahir, A. A., Chevallier, P., Arnaud, Y., and Ahmad, B.: Snow cover dynamics and hydrological regime of the Hunza River basin, Karakoram Range, Northern Pakistan, Hydrol. Earth Syst. Sci., 15, 2275–2290, https://doi.org/10.5194/hess-15-2275-2011, 2011.

USACE: Snow hydrology: Summary report of the snow investigations, https://usace.contentdm.oclc.org/digital/collection/p266001coll1/id/4172/, 1956.

USACE: Runoff from Snowmelt, https://www.publications.usace.army.mil/Portals/76/Publications/EngineerManuals/EM_1110-2-1406.pdf, 31 March 1998.

Walter, M. T., Brooks, E. S., McCool, D. K., King, L. G., Molnau, M., and Boll, J.: Process-based snowmelt modeling: does it require more input data than temperature-index modeling, Journal of hydrology, v. 300, 65–75, 2005.

Warren, S. G.: Optical properties of snow, Rev. Geophys., 20, 67, https://doi.org/10.1029/RG020i001p00067, 1982.

Warren, S. G. and Wiscombe, W. J.: A Model for the Spectral Albedo of Snow. II: Snow Containing Atmospheric Aerosols, J. Atmos. Sci., 37, 2734–2745, https://doi.org/10.1175/1520-0469(1980)037<2734:AMFTSA>2.0.CO;2, 1980.

Wiscombe, W. J. and Warren, S. G.: A Model for the Spectral Albedo of Snow. I: Pure Snow, J. Atmos. Sci., 37, 2712–2733, https://doi.org/10.1175/1520-0469(1980)037<2712:AMFTSA>2.0.CO;2, 1980.

Zhang, Y., Liu, S., Xie, C., and Ding, Y.: Application of a degree-day model for the determination of contributions to glacier meltwater and runoff near Keqicar Baqi glacier, southwestern Tien Shan, Ann. Glaciol., 43, 280–284, https://doi.org/10.3189/172756406781812320, 2006.